

2012

Vortex-Induced Vibrations of an Inclined Cylinder in Flow

Anil B. Jain

University of Massachusetts Amherst

Follow this and additional works at: <https://scholarworks.umass.edu/theses>



Part of the [Ocean Engineering Commons](#)

Jain, Anil B., "Vortex-Induced Vibrations of an Inclined Cylinder in Flow" (2012). *Masters Theses 1911 - February 2014*. 911.
Retrieved from <https://scholarworks.umass.edu/theses/911>

This thesis is brought to you for free and open access by ScholarWorks@UMass Amherst. It has been accepted for inclusion in Masters Theses 1911 - February 2014 by an authorized administrator of ScholarWorks@UMass Amherst. For more information, please contact scholarworks@library.umass.edu.

**VORTEX-INDUCED VIBRATIONS OF AN INCLINED CYLINDER IN
FLOW**

A Thesis Presented

by

ANIL B. JAIN

Submitted to the Graduate School of the
University of Massachusetts Amherst in partial fulfillment
of the requirements for the degree of

Master of Science in Mechanical Engineering

September 2012

© Copyright by Anil Jain 2012

All Rights Reserved

VORTEX-INDUCED VIBRATIONS OF AN INCLINED CYLINDER IN FLOW

A Thesis Presented

by

ANIL B. JAIN

Approved as to style and content by:

Yahya Modarres-Sadeghi, Chairperson

Jonathan P. Rothstein, Member

Yossi Chait, Member

Donald L. Fisher, Department Head
Mechanical and Industrial Engineering

ACKNOWLEDGEMENTS

I would like to dedicate this thesis to my parents, brother and sister, for their support throughout my life.

I would like to gratefully appreciate my advisor Dr. Yahya Modarres-Sadeghi for his continuous support during this study. His knowledge in vortex-Induced vibration was highly accessible to me. Also, special thanks to Prof. Jonathan Rothstein and Prof. Yossi Chait for being a part my thesis committee and providing me with useful comments.

I am thankful to Rick Winn and Al Rakouskas for their help in setting up the experimental setup. I will cherish the time spent at University of Massachusetts, Amherst thanks to all the lab-mates, professors, staffs and friends.

ABSTRACT

VORTEX-INDUCED VIBRATIONS OF INCLINED CYLINDERS IN FLOW

SEPTEMBER 2012

ANIL B. JAIN, B.S., UNIVERSITY OF MUMBAI, INDIA

M. S., UNIVERSITY OF MASSACHUSETTS AMHERST

Directed by: Professor Yahya Modarres-Sadeghi

When a bluff body is placed in flow, vortices are shed downstream of the body. For the case of a bluff body with a circular cross-section (a cylinder) attached to a spring and a damper, when the frequency of vortex shedding is close to the natural frequency of the structure, the cylinder oscillates in a direction perpendicular to the flow. This is called Vortex Induced Vibration (VIV) and is a canonical problem in fluid-structure interactions. The majority of studies on VIV of a flexibly mounted rigid cylinder are for the cases where the flow direction is perpendicular to the long axis of the structure. However, in many engineering applications, such as cable stays in bridges, mooring lines of floating offshore wind turbines and undersea pipelines, the flow direction may not be perpendicular to the structure. The hypothesis is that the VIV in inclined cylinders is similar to a normal-incidence case, if only the component of the free stream velocity normal to the cylinder axis is considered. This is called the Independence Principle (IP). The IP neglects the effect of the axial component of the flow, which is legit for small angles of inclination, but not for large angles. In this Thesis, a series of experiments have been conducted on a flexibly-mounted rigid cylinder placed inclined to the oncoming flow with various angles of inclination ($0^\circ < \theta < 75^\circ$) in a subcritical Reynolds number

range of 500 – 4,000 to investigate how the angle of inclination affects VIV. In these experiments, a rigid cylinder was mounted on springs, and air bearings were used to reduce the structural damping of the system. The system was placed in the test section of a recirculating water tunnel and crossflow displacements were measured. Even at high angles of inclination, large-amplitude oscillations were observed. The IP was found to be valid for angles of inclination up to 55° . While for all inclinations the onset of lock-in was observed to be at the same normalized flow velocity, for angles of inclination larger than 55° , the lock-in region (the range of dimensionless flow velocities for which the cylinder oscillates with a large amplitude) was smaller. These results show that the influence of the axial component of the flow is non-negligible for angles of inclination larger than 55° .

TABLE OF CONTENTS

	Page
ACKNOWLEDGEMENTS.....	iv
ABSTRACT.....	v
LIST OF TABLES.....	ix
LIST OF FIGURES.....	x
CHAPTER	
1. INTRODUCTION.....	1
1.1. Vortex Shedding.....	1
1.2. Vortex Induced Vibrations (VIV).....	2
2. BACKGROUND.....	7
2.1. A flexibly mounted rigid cylinder placed perpendicular to the flow.....	7
2.1.1. High mass-damping system.....	7
2.1.2. Low mass-damping system.....	9
2.1.2.1. Amplitude response of low mass-damping system.....	10
2.1.2.2. Frequency response of low mass-damping system.....	12
2.1.2.3. Fluid forces in low mass-damping system.....	13
2.2. Effect of the end conditions on VIV of vertical cylinder.....	15
2.3. Vortex induced vibrations of inclined cylinders.....	16
2.3.1. Amplitude and frequency response of flexibly mounted inclined cylinders.....	24
2.3.2. Fluid forces on flexibly mounted inclined cylinders.....	25
2.3.3. Independence Principle (IP).....	26
3. EXPERIMENTAL SETUP AND RESULTS.....	31
3.1. Experimental Setup.....	31
3.2. Experimental Results.....	33
3.2.1. VIV of vertical and inclined cylinders.....	33
3.2.2. Effect of mass ratio on VIV of inclined cylinders.....	46
3.2.3. Effect of positive and negative angle on VIV of inclined cylinders.....	50
3.2.4. Flow Visualization.....	54

TABLE OF CONTENTS

	Page
4. CONCLUSIONS	56
BIBLIOGRAPHY.....	58

LIST OF TABLES

	Page
Table 1. Nomenclature.....	6
Table 2. Enlisting the research work done on inclined cylinder.....	29
Table 3. Peak amplitudes for different angles of inclination	44

LIST OF FIGURES

	Page
Figure 1. Vortex formation behind a cylinder (Gerrard, 1966).	1
Figure 2. A rigid cylinder mounted on a spring-damper system and subjected to flow.	3
Figure 3. Oscillation characteristics for a freely vibrating circular cylinder in air with $m^*\zeta \sim 0.36$. o, vortex-shedding frequency; +, cylinder frequency; \square , phase angle; \times , oscillation amplitude; ϕ° , phase angle between fluid force and cylinder's displacement; f_v , vortex shedding frequency; f , oscillating frequency of cylinder; U , free stream velocity; St , Strouhal number for fixed cylinder (Feng 1968) (Figure from Bearman, 1984).	9
Figure 4. The amplitude response of flexibly mounted cylinder (\blacksquare) Khalak and Williamson (1997b) with $m^*\zeta = 0.013$ in water and (\diamond) Feng (1968) with $m^*\zeta = 0.36$ in air (Figure from Khalak and Williamson, 1997b).	10
Figure 5. Amplitude response for $m^*\zeta = 0.0014$ (\bullet) and 0.0032 (\circ) (Govardhan and Williamson, 2000) and $m^*\zeta = 0.00016$ (red dots) (Brankovic and Bearman, 2006) (Figure from Brankovic and Bearman, 2006).	11
Figure 6. Peak amplitude of the upper and lower branch at different $m^*\zeta$ parameter. (\blacksquare), peak upper branch amplitude (Khalak and Williamson, 1997a); (\blacktriangle), peak lower branch amplitude (Khalak and Williamson, 1997a); (\circ), peak amplitude (Griffin, 1980) (Figure from Khalak and Williamson, 1997a).	12
Figure 7. Frequency response $f^* = f/f_N$ for $m^*\zeta = 0.013$. The U^* and f^* are formed using f_N in water (Figure from Khalak and Williamson, 1997a).	12
Figure 8. Classical lock-in phenomenon observed for different mass ratios, $m^*=10.3$ ($m^*\zeta = 0.017$) and 20.6 ($m^*\zeta = 0.019$) (Figure from Khalak and Williamson, 1997a).	13
Figure 9. Lift coefficient C_L and drag coefficient C_D versus reduced velocity U^* for $m^*=10.1$ and $m^*\zeta= 0.013$ (Figure from Khalak and Williamson, 1997b).	14
Figure 10. Cylinders with different types of end conditions (Figure from Morse et al., 2008).	15

Figure 11. Cylinder placed inclined with respect to the incoming flow along with the normal and tangential components of flow velocity.....	16
Figure 12. Normalized Strouhal number for fixed cylinder with different angles of Inclination. 90° corresponds to vertical cylinder in the plot. (Figure from Surry and Surry, 1967).....	17
Figure 13. Flow visualization behind a fixed inclined cylinder in a wind tunnel (Ramberg, 1983) (Figure from Thakur et al., 2004).....	18
Figure 14. r.m.s. (η_{rms}) and maximum (η_{max}) amplitude versus reduced velocity. In this plot A^* is represented by η (Figure from Lucor and Karniadakis, 2003).....	19
Figure 15. Mean drag coefficient ($C_{D(mean)}$) versus reduced velocity (Figure from Lucor and Karniadakis, 2003).....	20
Figure 16. r.m.s. lift coefficient ($C_{L(r.m.s.)}$) versus reduced velocity (Figure from Lucor and Karniadakis, 2003).....	21
Figure 17. Vortex shedding behind an inclined cylinder towed in a tank for (a) 0°, (b) 30° and (c) 60° (Figure from Thakur et al., 2004).....	22
Figure 18. Influence of angle of Inclination on (a) Strouhal number, (b) Drag Coefficient, (c) Lift coefficient; (d), (e) and (f) the ratio of normalized coefficients after applying the IP to actual coefficients (Figure from Willden and Guerbi, 2010).....	23
Figure 19. A^* plotted against U^* for 0° (●), 20° (▲) and 45° (■) for $m^*\zeta = 0.0125$ (Reproduced from Franzini et al, 2009).....	24
Figure 20. Non-dimensional frequency f^* versus the reduced velocity U^* for 0° (●), 20° (▲) and 45° (■) for $m^*\zeta = 0.0125$ (Reproduced from Franzini et al, 2009).....	25
Figure 21. Lift coefficient $C_{L(rms)}$ versus the reduced velocity U^* for 0° (●), 20° (▲) and 45° (■) for $m^*\zeta = 0.0125$ (Reproduced from Franzini et al., 2009).....	26
Figure 22. Drag coefficient C_D versus the reduced velocity U^* for 0° (●), 20° (▲) and 45° (■) for $m^*\zeta = 0.0125$ (Reproduced from Franzini et al., 2009).....	26
Figure 23. Non-dimensional A^* versus normal reduced velocity U_n^* after applying the IP for 0° (●), 20° (▲) and 45° (■) for $m^*\zeta = 0.0125$ (Reproduced from Franzini et al., 2009).....	27

Figure 24. Non-dimensional frequency f^* versus the normal reduced velocity U_n^* after applying the IP for 0° (●), 20° (▲) and 45° (■) for $m^*\zeta = 0.0125$ (Reproduced from Franzini et al., 2009).....	27
Figure 25. Drag coefficient C_D versus the normal reduce velocity U_n^* after applying the IP for 0° (●), 20° (▲) and 45° (■) for $m^*\zeta = 0.0125$ (Reproduced from Franzini et al., 2009).....	28
Figure 26. Lift coefficient $C_{L(rms)}$ versus the normal reduced velocity U_n^* after applying the IP for 0° (●), 20° (▲) and 45° (■) for $m^*\zeta = 0.0125$ (Reproduced from Franzini et al., 2009).....	28
Figure 27. Experimental Setup.	31
Figure 28. Decay test in air.	32
Figure 29. (a) Comparison of our results for a normal incidence cylinder ($m^*\xi = 0.029$) with 1mm gap ($0.08D$) with Khalak & Williamson's (1999) results ($m^*\xi = 0.013$). (b) Frequency response for a normal-incidence cylinder ($m^*\xi = 0.029$).	35
Figure 30. (a) Amplitude and (b) Frequency response for a 20° -inclined cylinder with 1mm gap ($0.08D$), compared with our vertical cylinder results ($m^*\xi = 0.029$) and Franzini et al. (2009) ($m^*\xi = 0.0125$).	36
Figure 31. (a) Amplitude and (b) Frequency response for a 45° -inclined cylinder with 1mm gap ($0.08D$), compared with our vertical cylinder results ($m^*\xi = 0.029$) and Franzini et al. (2009) ($m^*\xi = 0.0125$).	38
Figure 32. (a) Amplitude and (b) Frequency response for a 55° -inclined cylinder with 1mm gap ($0.08D$).	39
Figure 33. Various runs showing (a) Amplitude and (b) Frequency response for a 65° -inclined cylinder with 1mm gap ($0.08D$).	41
Figure 34. (a) Amplitude and (b) Frequency response for a 75° -inclined cylinder with 1mm gap ($0.08D$).	42
Figure 35. (a) Amplitude and (b) Frequency response for all the angle of inclination with 1mm gap ($0.08D$) and $m^*\xi = 0.029$	43
Figure 36. (a) Amplitude and (b) Frequency response for all the angle of inclination after applying Independence Principle ($U_n^* = U^* \cos\theta$) with 1mm gap ($0.08D$) and $m^*\xi = 0.029$	45

Figure 37. Comparison of (a) Amplitude and (b) Frequency response for 45°-inclined cylinder with $m^*= 6.5$ ($m^*\zeta= 0.029$) and $m^*= 13$ ($m^*\zeta= 0.0585$) with 1mm gap ($0.08D$).	47
Figure 38. Comparison of (a) Amplitude and (b) Frequency response for 65°-inclined cylinder with $m^*= 6.5$ ($m^*\zeta= 0.029$) and $m^*= 13$ ($m^*\zeta= 0.0585$) with 1mm gap ($0.08D$).	48
Figure 39. (a) Amplitude and (b) Frequency response after applying IP to 45° and 65°-inclined cylinder with $m^*= 13$ ($m^*\zeta= 0.0585$).	49
Figure 40. Comparison of (a) Amplitude and (b) Frequency response for $\pm 45^\circ$ -inclined cylinder with 1mm gap ($0.08D$) and $m^*\zeta= 0.029$.	51
Figure 41. Comparison of (a) Amplitude and (b) Frequency response for $\pm 65^\circ$ -inclined cylinder with 1mm gap ($0.08D$) and $m^*\zeta= 0.029$.	52
Figure 42. (a) Amplitude and (b) Frequency response after applying IP to -45° and -65° -inclined cylinder with $m^*= 6.5$ ($m^*\zeta= 0.029$).	53
Figure 43. Flow visualization in the wake of (a) Vertical cylinder, (b) 45°-inclined cylinder and (c) 65°-inclined cylinder Flow is from left to right.	55

CHAPTER 1

INTRODUCTION

1.1. Vortex Shedding

When a cylinder is placed in flow, shear layers are formed because of the separation of the boundary layer around the cylinder. The strength of the shear layer increases away from the cylinder and it continues to grow until a stronger opposing shear layer breaks off the former shear layer and results in vortex shedding downstream of the cylinder (Bearman, 1984). This repeated action results in Von Karman Vortex street. The number of vortices shed per unit time is called the frequency of vortex shedding and is non-dimensionalized through the definition of the Strouhal number:

$$St = \frac{f_v D}{U} \quad (1.1)$$

where, f_v is the frequency of vortex shedding behind the cylinder.

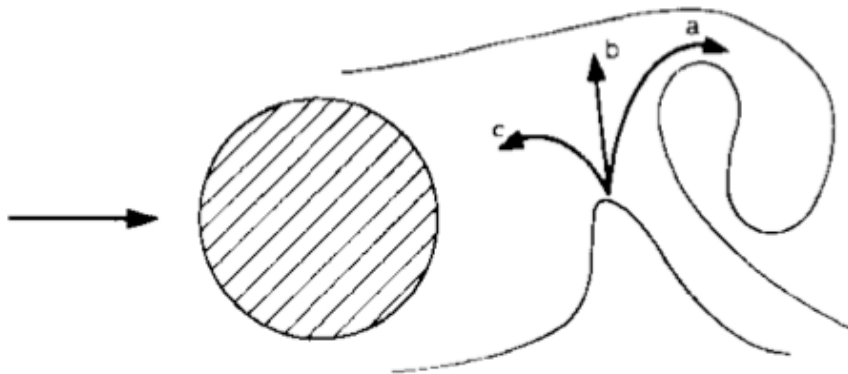


Figure 1. Vortex formation behind a cylinder (Gerrard, 1966).

The formation of vortex behind a circular cylinder in a flow can be shown using Gerrard's (1966) sketch shown in Figure 1. As the separation takes place, the fluid (a) grows bigger and fluid (b) finds its way into the developing shear layer. The fluid (c) from the base of the cylinder entrains into fluid (b), increasing its size. Thus, two opposing signed vortices are formed and keep on drifting downwards away from the cylinder (Bearman, 1984).

1.2. Vortex Induced Vibrations (VIV)

When a flexibly mounted rigid cylinder is placed in flow, vortices are shed downstream of the cylinder. The shed vortices result in an oscillatory external force exerted on the cylinder. Consequently, the cylinder oscillates transverse to the flow direction. This is called Vortex Induced Vibration (VIV). The amplitude of VIV for a cylinder placed in flow can reach up to around one diameter of the cylinder in the transverse direction.

Rigid structures with circular cross-sections are used extensively to study VIV, because of their various engineering applications. The system can be represented by a linear mass-spring-damper system as shown in Figure 2, in which a rigid cylinder with diameter D and length L , is supported by a spring with stiffness k and a damper with damping c . The cylinder is placed perpendicular to the flow with a velocity U and density ρ .

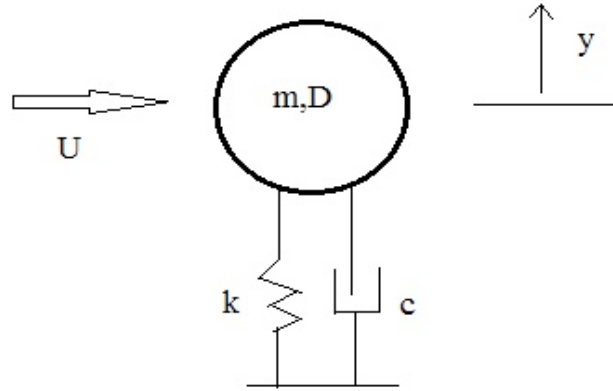


Figure 2. A rigid cylinder mounted on a spring-damper system and subjected to flow.

The equation of motion generally used to represent the oscillations of a cylinder in the transverse direction is the linear equation of a mass-spring-damper system, which is subjected to an external force due to the flow, and reads as:

$$m \ddot{y} + c \dot{y} + ky = F_Y, \quad (1.2)$$

where, m is the mass per unit length of the cylinder, y is the cylinder position measured from rest, k is the spring stiffness, c is the structural damping and F_Y is the corresponding fluctuating transverse fluid force called lift force. The fluctuating lift force can be expressed in terms of the lift coefficient C_Y where:

$$C_Y = \frac{F_Y}{\frac{1}{2} \rho U^2 DL}, \quad (1.3)$$

Assuming that the cylinder's displacement has a sinusoidal form:

$$y(t) = y_0 \sin(\omega t), \quad (1.4)$$

The fluid force leads the displacement of the cylinder by a phase angle f and is given by:

$$F_Y(t) = F_0 \sin(\omega t + \phi), \quad (1.5)$$

where, $w = 2pf$ and f is the body oscillation frequency. From equations 1.2-1.5, the non-dimensional amplitude and frequency can be derived as (Govardhan and Williamson, 2000):

$$A^* = \frac{1}{4\pi^3} \frac{C_Y \sin \phi}{(m^* + C_A)\xi} \left(\frac{U^*}{f^*} \right)^2 f^*, \quad (1.6)$$

$$f^* = \sqrt{\frac{m^* + C_A}{m^* + C_{EA}}}. \quad (1.7)$$

In these equations,

$$A^* = \frac{A}{D} \quad (1.8)$$

is the dimensionless amplitude (A is the amplitude of oscillation);

$$f^* = \frac{f}{f_N} \quad (1.9)$$

is the dimensionless frequency (f is the oscillating frequency of the cylinder and f_N is the natural frequency of the system in water);

$$U^* = \frac{U}{f_N D} \quad (1.10)$$

is the reduced velocity;

$$m^* = \frac{m}{\frac{1}{4} \pi \rho D^2 L} \quad (1.11)$$

is the mass ratio, which is the ratio of the cylinder mass (or moving mass) to the mass of the displaced fluid (m_d);

$$m_A = C_A m_d \quad (1.12)$$

is the added mass and $m_d = \rho r D^2 L / 4$ is the displaced fluid mass. C_A is the potential added mass coefficient in otherwise still fluid. A nominal value for the added mass (C_A) is

usually assumed to be 1;

$$C_{EA} = \frac{1}{2\pi^3} \frac{C_Y \cos \phi}{A^*} \left(\frac{U^*}{f^*} \right)^2 \quad (1.13)$$

is the effective added mass coefficient. It includes the effect due to the total transverse fluid force in-phase with the body acceleration ($C_Y \cos \phi$), and

$$\zeta = \frac{\delta}{\sqrt{(2\pi)^2 + \delta^2}} \quad (1.14)$$

is the structural damping (δ is the logarithmic decrement).

Table 1 summarizes the parameters used in this Thesis.

Table 1. Nomenclature

Amplitude ratio (A^*)	$A^* = \frac{A}{D}$
Damping ratio (ζ)	$\zeta = \frac{\delta}{\sqrt{(2\pi)^2 + \delta^2}}$
Frequency ratio (f^*)	$f^* = \frac{f}{f_N}$
Natural frequency (f_N)	$f_N = \frac{1}{2\pi} \sqrt{\frac{k}{m + m_A}}$
Reynolds number (Re)	$Re = \frac{UD}{\nu}$
Strouhal number (St)	$St = \frac{f_v D}{U}$
Normalized reduced velocity (U_n^*)	$U_n^* = \frac{U \cos \theta}{f_N D}$
Reduced velocity (U^*)	$U^* = \frac{U}{f_N D}$
Lift coefficient (C_L)	$C_L = \frac{F_L}{\frac{1}{2} \rho U^2 DL}$
Drag coefficient (C_D)	$C_D = \frac{F_D}{\frac{1}{2} \rho U^2 DL}$
Mass ratio (m^*)	$m^* = \frac{m}{\frac{1}{4} \pi \rho D^2 L}$
Potential added mass coefficient (C_A)	$m_A = C_A m_d$
Effective added mass coefficient (C_{EA})	$C_{EA} = \frac{1}{2\pi^3} \frac{C_Y \cos \phi}{A^*} \left(\frac{U^*}{f^*} \right)^2$
Phase angle (ϕ°)	$\phi^\circ = \tan^{-1} \left[\frac{2\zeta \frac{f}{f_N}}{1 - \left(\frac{f}{f_N} \right)^2} \right]$

CHAPTER 2

BACKGROUND

Since the discovery of formation of vortices produced by translating rods through air by Strouhal (1878) and the analysis of stability of vortex street configurations by Von Karman (1912), the problem of VIV has been studied comprehensively. Some of the important work done in the field of VIV on normal incident and inclined rigid cylinder with only one degree of freedom (crossflow) are discussed in the following sections.

2.1. A flexibly mounted rigid cylinder placed perpendicular to the flow

A flexibly mounted rigid cylinder placed in flow can oscillate in both the streamwise (inline) and crossflow direction. In general the amplitude of oscillation in the inline direction is much smaller than that in the crossflow direction. Due to the nature of vortex shedding, the frequency of oscillation in the inline direction is twice the frequency of oscillation in the crossflow direction. The amplitude of cross flow VIV can be as large as 1-1.2 times the cylinder diameter.

The dynamics of the system varies dramatically depending on the mass-damping factor, which is defined as $m^*\zeta$ (see equations 1.11 and 1.14). In the following sections, we discuss the system response with high and small mass-damping factors.

2.1.1. High mass-damping system

The early studies on VIV were based on the experiments in the wind tunnel with relatively high mass ratios and damped systems, resulting in large mass-damping parameters. The purpose of these studies was to understand the VIV of the structures in

wind such as bridges and chimneys.

An important study by Feng (1968) provided a comprehensive analysis of the amplitude and frequency response of the cylinder oscillating in the transverse direction. Figure 3 shows the non-dimensional amplitude (A^*) and non-dimensional frequency plotted against reduced velocity (U^*) (defined in equation 1.10). It can be seen that, initially, as the velocity (U) is increased from zero, the cylinder is stationary and the vortex shedding frequency (f_V) follows the straight line of Strouhal number relation ($St = 0.198$), similar to the fixed cylinder. As the flow velocity increases, the vortex shedding frequency (f_V) approaches the natural frequency (f_N) of the system ($f_V \sim f_N$), and it no longer follows the Strouhal number's straight line. At this velocity, the cylinder starts oscillating in the crossflow direction. In fact, the vortex shedding gets locked in with the natural frequency of the cylinder and collapses into a single frequency. This is called "lock-in" phenomenon in Feng's experiment. The maximum amplitude of $0.55D$ (D is the cylinder diameter) was achieved at a reduced velocity of 6.3. The arrows show the effect of hysteresis, depending on the approach to the lock-in range - whether from a low velocity or from a high velocity. The phase angle (phase difference between the leading fluctuating lift force and cylinder's displacement) against the reduced velocity shows a hysteresis effect as well.

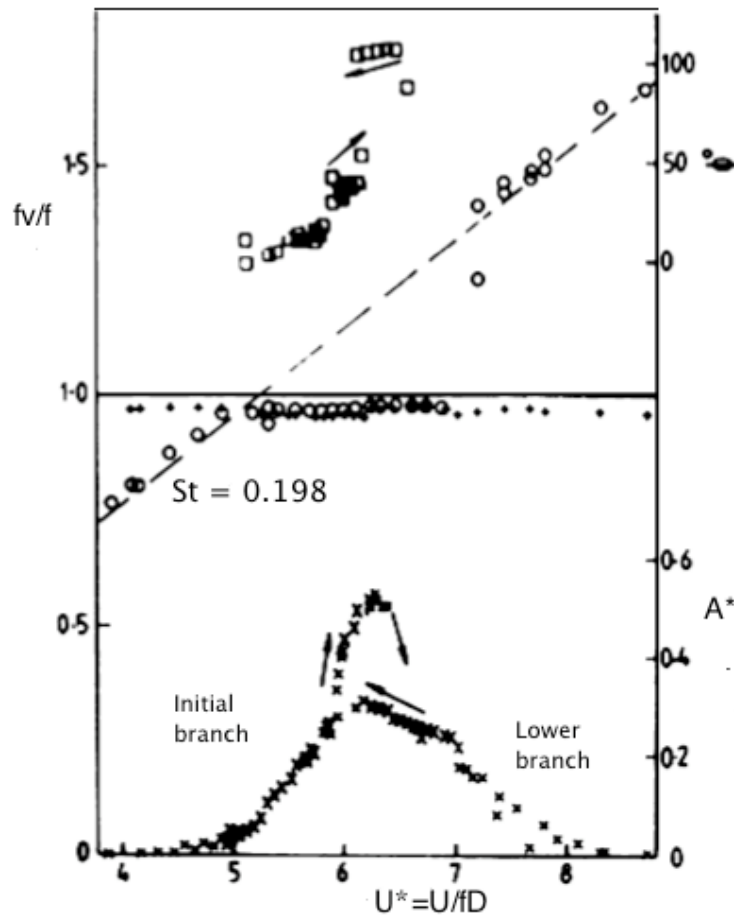


Figure 3. Oscillation characteristics for a freely vibrating circular cylinder in air with $m^*\xi \sim 0.36$. \circ , vortex-shedding frequency; $+$, cylinder frequency; \square , phase angle; \times , oscillation amplitude; ϕ° , phase angle between fluid force and cylinder's displacement; f_v , vortex shedding frequency; f , oscillating frequency of cylinder; U , free stream velocity; St , Strouhal number for fixed cylinder (Feng 1968) (Figure from Bearman, 1984).

2.1.2. Low mass-damping system

When a cylinder is placed in water and air bearings are used to reduce the structural damping, the setup can be considered as low mass-damping system. "Studying such systems is important because they have conditions similar to those of the offshore structures" (Khalak and Williamson, 1996).

2.1.2.1. Amplitude response of low mass-damping system

Khalak and Williamson (1996) studied the VIV of flexibly mounted cylinder with very low mass-damping system - almost an order of magnitude smaller than previously conducted experiments such as Feng's (1968).

The effect of $m^*\zeta$ on the system's response can be seen in Figure 4 where Khalak & Williamson's (1997b) and Feng's (1968) data are plotted. As the $m^*\zeta$ becomes smaller (3% of Feng's value), the lock-in range increases by four fold and higher peak amplitudes are observed (twice the peak amplitude of Feng's experiment). Another important observation is the appearance of a third branch called the "upper branch" in comparison with the other two branches (initial and lower) seen in Feng's results. It should be noted that in calculating the added mass, m_A , the added mass coefficient, C_A , is assumed to be equal to 1, instead of the effective added mass coefficient, C_{EA} , which can be calculated by taking into account the total transverse fluid force in-phase with the cylinder's acceleration.

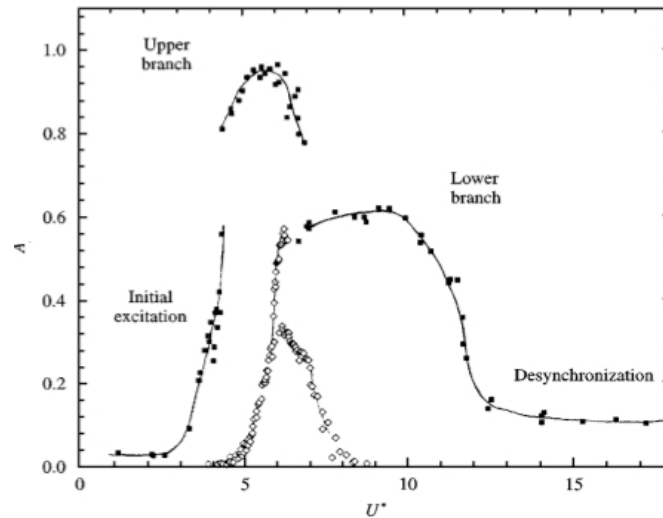


Figure 4. The amplitude response of flexibly mounted cylinder (■) Khalak and Williamson (1997b) with $m^*\zeta = 0.013$ in water and (◇) Feng (1968) with $m^*\zeta = 0.36$ in air (Figure from Khalak and Williamson, 1997b).

Brankovic and Bearman (2006) and Govardhan and Williamson (2000) measured the transverse oscillations for even smaller $m^*\zeta$ (Figure 5). The peak amplitude attains a value of around 1.2, which is higher than Khalak and Williamson (1997b) values.

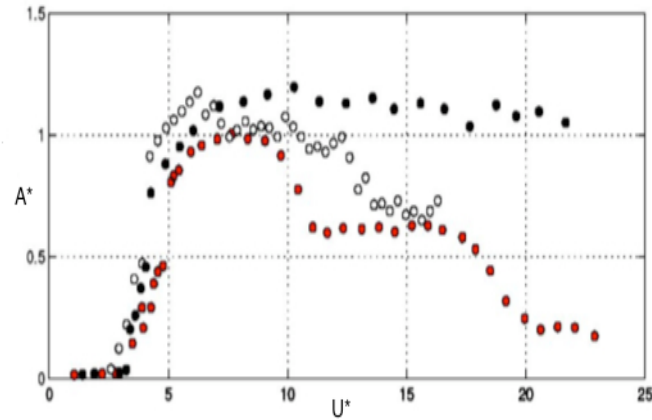


Figure 5. Amplitude response for $m^*\zeta = 0.0014$ (●) and 0.0032 (○) (Govardhan and Williamson, 2000) and $m^*\zeta = 0.00016$ (red dots) (Brankovic and Bearman, 2006) (Figure from Brankovic and Bearman, 2006).

Khalak and Williamson (1997a) showed that the magnitude of peak amplitude in the upper branch depends on the combined value of $m^*\zeta$ of the system (Figure 6), whereas the lower branch response seems to be independent from the mass-damping parameter. On the other hand, the relatively higher $m^*\zeta$ used in the experiments performed by Griffin (1980) reveals the absence of upper branch and relatively smaller amplitude response.

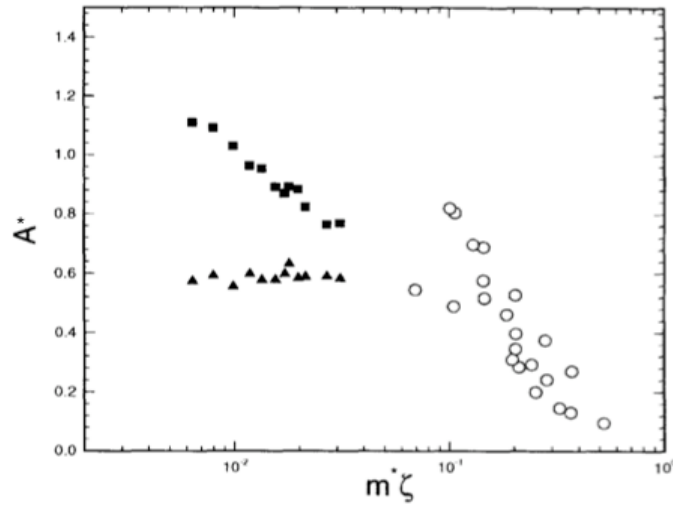


Figure 6. Peak amplitude of the upper and lower branch at different $m^*\zeta$ parameter. (■), peak upper branch amplitude (Khalak and Williamson, 1997a); (▲), peak lower branch amplitude (Khalak and Williamson, 1997a); (○), peak amplitude (Griffin, 1980) (Figure from Khalak and Williamson, 1997a).

2.1.2.2. Frequency response of low mass-damping system

Khalak and Williamson (1997a) measured the frequency response (f^* = oscillating frequency (f) / natural frequency of the system (f_N)) against the reduced velocity (U^*) for $m^*\zeta = 0.013$ ($m^* = 2.4$). As it can be seen in Figure 7, f^* reaches a value of 1.5 and higher, which is very high compared to the values observed for f^* in the case of high $m^*\zeta$.

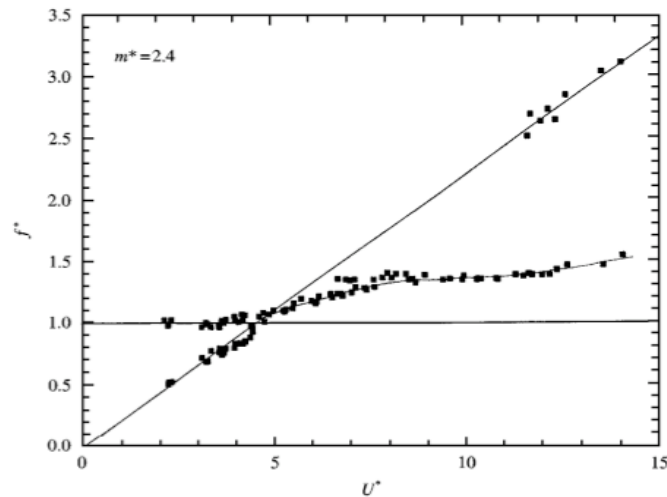


Figure 7. Frequency response $f^* = f/f_N$ for $m^*\zeta = 0.013$. The U^* and f^* are formed using f_N in water (Figure from Khalak and Williamson, 1997a).

The difference in frequency response for systems with low and high mass ratios (when $m^*\zeta = \text{constant}$) is because of the effect of the added mass (m_A), which decreases as the reduced velocity increases and thus resulting in an increase in natural frequency according to the following equation:

$$f_N = \frac{1}{2\pi} \sqrt{\frac{k}{m + m_A}}. \quad (2.1)$$

Therefore, the low m^* cylinders (Figure 7) have broader range of lock-in compared to high mass-ratio cylinders (Figure 8). The effect of added mass for high m^* cylinder is not as significant, resulting in narrower range of lock-in (Vikestad et al., 2000). The classical lock-in phenomenon can be seen for larger mass ratios as well, as predicted by Bearman (1984) and shown by Khalak and Williamson (1997a) in Figure 8.

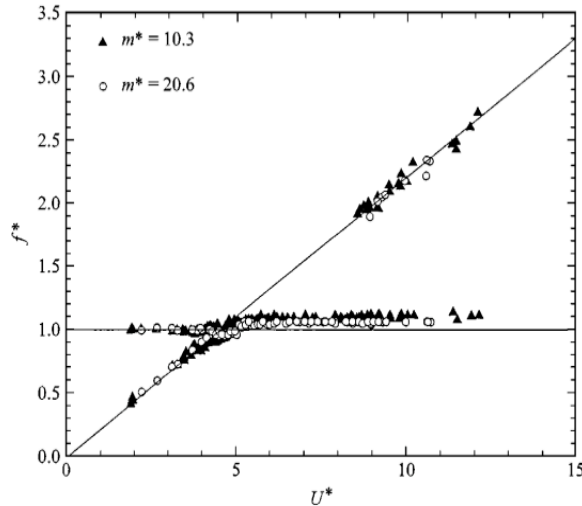


Figure 8. Classical lock-in phenomenon observed for different mass ratios, $m^*=10.3$ ($m^*\zeta = 0.017$) and 20.6 ($m^*\zeta = 0.019$) (Figure from Khalak and Williamson, 1997a).

2.1.2.3. Fluid forces in low mass-damping system

Khalak and Williamson (1997b) measured the lift coefficient ($C_{L(r.m.s.)}$) and drag coefficient (C_D) by normalizing the forces by $\frac{1}{2}\rho U^2 DL$, where L and D are the immersed

length and diameter of the cylinder respectively, ρ is the fluid density, and U is the fluid velocity.

Figure 9 shows a maximum C_D of 5.2 with mean C_D of around 3.5. This is three-fold increase over the stationary case. $C_{L(r.m.s.)}$ reaches 2, which corresponds to a maximum C_L of 3, five times increase over the stationary cylinder case. The jump between the initial and upper branch can be associated with the sharp peak in the lift coefficient, which occurs at the transition from the initial branch to the upper branch (Khalak and Williamson, 1997b).

“The force coefficients (drag and lift) and the vortex shedding frequency are independent from the Reynolds number (A dimensionless parameter characterizing different flow regimes, defined as $Re=UD/\nu$, where ν is the kinematic viscosity) as long as the latter is in the sub-critical regime ($300 < Re < 3 \times 10^5$)” (Schewe, 1983).

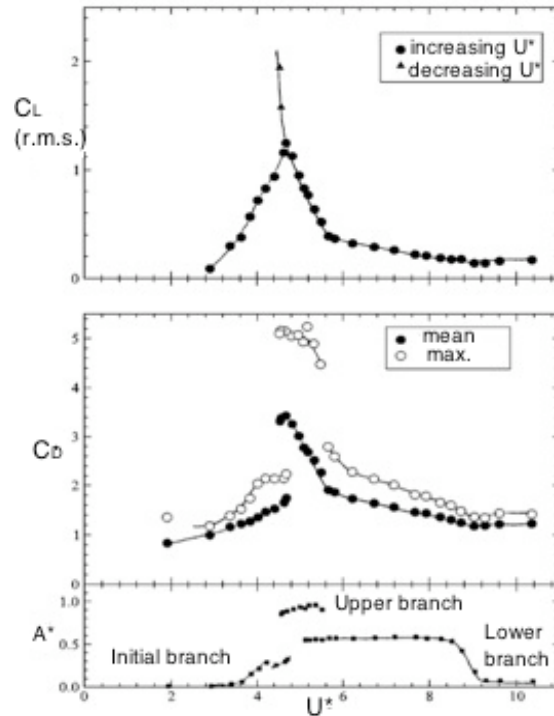


Figure 9. Lift coefficient C_L and drag coefficient C_D versus reduced velocity U^* for $m^*=10.1$ and $m^*\zeta=0.013$ (Figure from Khalak and Williamson, 1997b).

2.2. Effect of the end conditions on VIV of vertical cylinder

The end conditions of the cylinder play an important role in the observed VIV response of the cylinder. For a vertically suspended cylinder partially submerged in water, the upper end of the cylinder is in contact with free surface and the lower end is submerged in water. In order for the vortices shed downstream of the cylinder to remain parallel to the cylinder axis, three-dimensionality in the flow must be avoided. Three dimensionality can be induced in the flow if proper end conditions are not maintained. The free surface results in parallel shedding (Khalak and Williamson, 1996) but the lower end of the cylinder can induce three-dimensionality into the flow. Various types of end conditions used in the literature are listed below:

- a. Endplates attached to the test section with a small gap between the test cylinder end and the plate (Khalak and Williamson 1996,1997a, 1997b) (Figure 10a),
- b. Endplates attached to the cylinder (Stansby, 1974) (Figure 10b),
- c. Free end (Klamo, 2007) (Figure 10c),
- d. Free end close to the test section (Bearman and Brankovic, 2006 and Franzini et al., 2009) (Figure 10d).

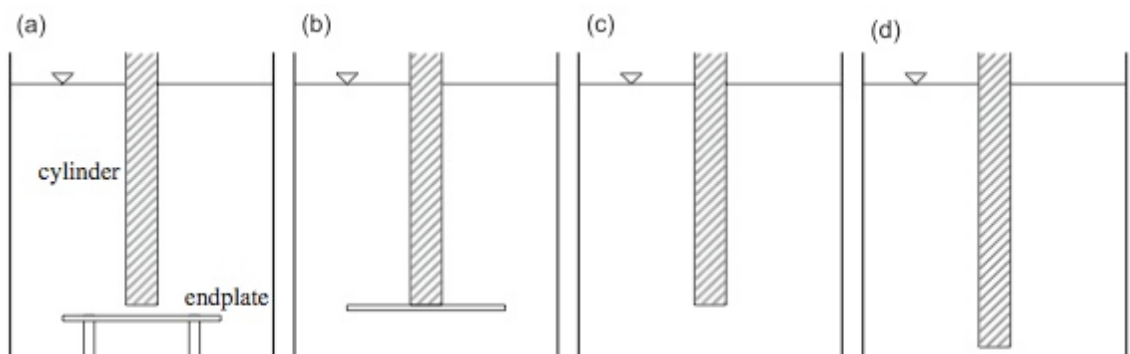


Figure 10. Cylinders with different types of end conditions (Figure from Morse et al., 2008).

Morse et al. (2008) showed that the cylinder with attached end plate and without attached end plate behave similarly if the gap between the cylinder end and the plate in the latter case is less than 15% of the cylinder's diameter. Cylinders with free end (gap more than $0.15D$) have same peak amplitude, when compared with cases (a) and (b) but there is no distinct upper and lower branch of oscillation. Case (d) works well if the gap is less than $0.15D$ but it relies on the properties of the boundary layer or turbulence inside the test section of the water tunnel.

2.3. Vortex induced vibrations of inclined cylinders

Despite the extensive research being conducted on the VIV of normal-incident cylinders, many questions are still unanswered in the case of inclined cylinders. There are significant conflicting reports on the characteristics of VIV in inclined cylinders.

A fixed inclined cylinder is considered to be similar to the normal-incidence case, through the use of the component of free stream velocity normal to the cylinder axis. This is called the Independence Principle (IP). The angle of inclination is defined as the angle between the cylinder axis and the vertical line if the flow is from left to right (Figure 11). Zero angle of inclination corresponds to a cylinder perpendicular to the incoming flow (cross-flow).

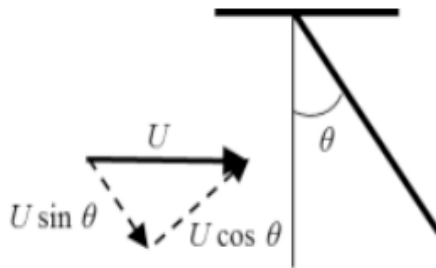


Figure 11. Cylinder placed inclined with respect to the incoming flow along with the normal and tangential components of flow velocity.

Surry and Surry (1967) performed wind tunnel experiments on fixed inclined cylinder at five different speeds covering the Reynolds number range of 4,500 - 63,000 for different angles of inclination ($\theta = 0^\circ, 16^\circ, 26^\circ, 38^\circ, 48^\circ$ and 55°) They found that the Strouhal number (St) based on the normal velocity component remains constant till $\theta = 40^\circ$ and 50° (Figure 12).

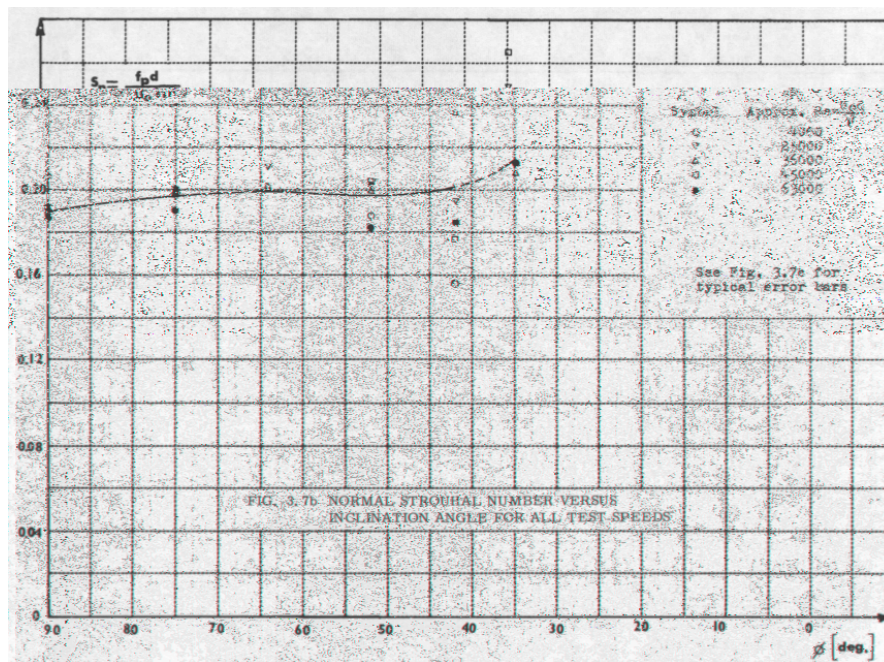


Figure 12. Normalized Strouhal number for fixed cylinder with different angles of Inclination. 90° corresponds to vertical cylinder in the plot. (Figure from Surry and Surry, 1967).

King (1977) investigated VIV of inclined circular cylinders in the subcritical Re range of 2000-20,000 and for angles of inclination ranging from -45° to $+45^\circ$. He observed the maximum cross-flow amplitude in the range of normal reduced velocity ($U_n^* = U \cos \theta / f_N D$) of 5.8-7.0. He encountered relatively large oscillations for inclination angles of $+45^\circ$ and -45° and also showed that the response of the cylinder is the same for both the negative and positive angles of inclination. He found that the maximum

amplitude increases with an increase in inclination and attributed this phenomenon to the change in the immersed length.

Ramberg (1983) studied the effect of inclination angle for stationary and forced vibrating circular cylinders with aspect ratios 20-90 in the Re range of 150-1,100. A typical flow visualization result for a fixed inclined cylinder from Ramberg (1983) is shown in Figure 13. It can be seen that the vortices are parallel to each other but they are at an angle greater than the cylinder angle of inclination near the upstream end of the cylinder (θ_1 in Figure 13). But at a certain distance away from the cylinder the vortices are aligned at the same inclination as the cylinder (θ_2 in Figure 13). He determined that the results were affected by the end conditions, especially at low Reynolds numbers. He found that IP was not valid for stationary inclined cylinders because the shedding frequency was larger than what is expected by IP, whereas the shedding angle, the vortex-formation length, the base pressure and the wake width are all less when compared with a vertical cylinder in cross-flow with the same normal component of the free stream velocity. However, for the cylinders forced to oscillate in the Re range of 160-460, he found that the vortex shedding is parallel to the cylinder.

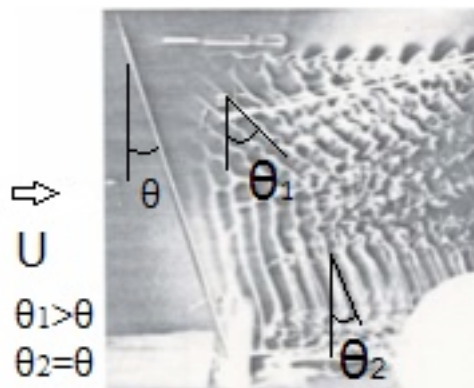


Figure 13. Flow visualization behind a fixed inclined cylinder in a wind tunnel (Ramberg, 1983) (Figure from Thakur et al., 2004).

Lucor and Karniadakis (2003) performed direct numerical simulations (DNS) to validate the Independence Principle for stationary and freely vibrating rigid cylinders for large angles of inclination ($\theta = -60^\circ$ and -70°) with $m^*\zeta = 0.006$ and an aspect ratio (L/D) of 22. For a freely vibrating rigid yawed cylinder (RYC in Figure 14), they observed large crossflow amplitude for large inclination angles. The amplitude of oscillation decreased as the angle of inclination was increased (Figure 14). For -70° angle ($Re = 1000$ or normalized Reynolds number $Re_n = Re \cos\theta = 342$), the maximum dimensionless amplitude of oscillation ($A^* = 0.52$) represented by case I (hollow triangle symbol), reached the value given by IP, when compared against the response of rigid cylinder normal to the incoming flow ($Re = 300$). The maximum A^* for cylinder with $\theta = -60^\circ$ was 0.63 represented by case II (hollow circular symbol), smaller than the value for the free cylinder at normal incidence at $Re = 1000$ ($A^* = 0.75$). (No exact comparison was available to validate IP but they compared with the normal incident cylinder at $Re = 300$. Re_n for -60° and -70° inclined cylinder are 500 and 342 respectively).

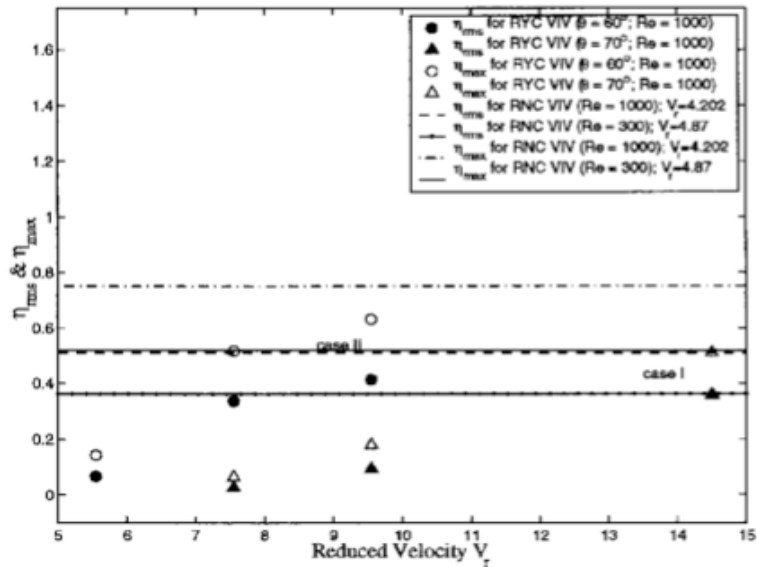


Figure 14. r.m.s. (η_{rms}) and maximum (η_{max}) amplitude versus reduced velocity. In this plot A^* is represented by η (Figure from Lucor and Karniadakis, 2003).

They showed that the vortex shedding behind the moving cylinder is parallel to the cylinder axis as long as the cylinder crossflow amplitude is not too small, and for zero cylinder response, the vortex shedding has a tendency to slant. For a stationary cylinder, they concluded that the IP is not valid for large angles of inclination (critical angle not discussed) and the vortex shedding angle (58°) is smaller than the angle of inclination. For the case of $\theta = -70^\circ$, the drag coefficient is higher than predicted by IP. For a -70° -inclined moving cylinder, the drag coefficients at reduced velocity $U^* = 14.5$ or $U_n^* = 4.95$ ($C_{D(mean)} \approx 1.9$) where lock-in occurs, are quite larger than predicted by IP ($C_{D(mean)} = 1$). Similarly, for the -60° yawed moving cylinder ($Re = 1000$ or $Re_n = 500$), the drag coefficient increases as the U^* increases and attains a value corresponding to a rigid normal cylinder (RNC) at $Re = 1000$, as shown in Figure 15.

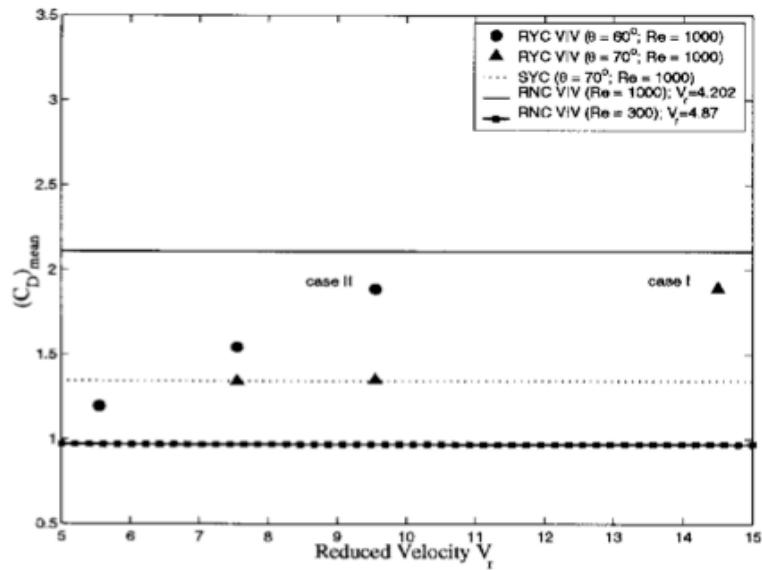


Figure 15. Mean drag coefficient ($C_{D(mean)}$) versus reduced velocity (Figure from Lucor and Karniadakis, 2003).

The lift coefficient $C_{L(r.m.s.)}$ (the hollow symbols are averaged over time whereas the solid symbols are averaged over the space) for the -70° -inclined moving cylinder is

close to the value predicted by the IP and for the -60° -inclined moving cylinder, $C_{L(r.m.s.)}$ is around 1 (Figure 16).

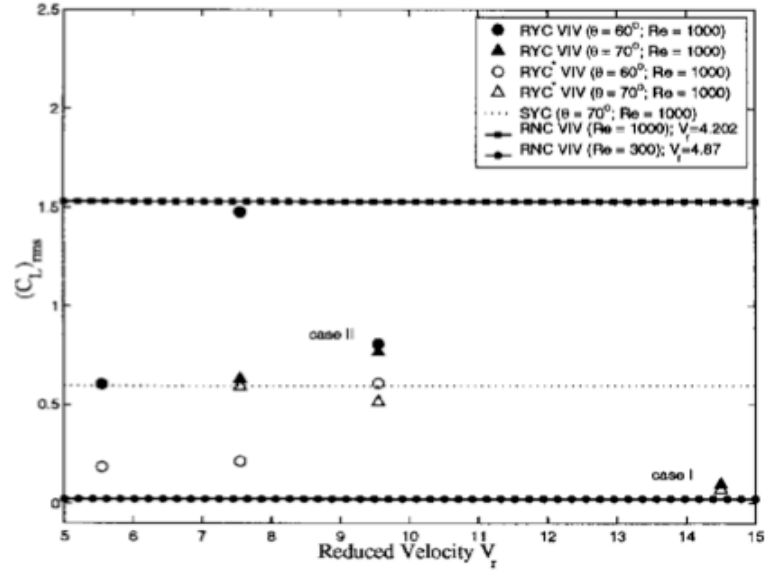


Figure 16. r.m.s. lift coefficient ($C_{L(r.m.s.)}$) versus reduced velocity (Figure from Lucor and Karniadakis, 2003).

Thakur et al. (2004) performed an experiment on yawed cylinder ($\theta = 30^\circ$ and 60°) by towing single and multiple cylinders in a tank and observed that the wake vortices approach the cylinder yaw angle sufficiently far away from the cylinder's upstream end, but the shedding angle closer to the cylinder's upstream end was smaller than the angle of yaw (Figure 17), opposite to Ramberg's results (1983) shown in Figure 13. Thakur et al. described the difference between the two cases was because of the difference in the experimental setup (cylinder was towed in his experiment). The Strouhal number, based on the normal towing velocity of the cylinder, increased with the angle of inclination (0.24 for 30° and 0.28 for 60°) in agreement with Van Atta's (1968) observation. Zhao et al. (2009) in their direct numerical simulation (DNS) found that for a fixed cylinder, the pressure coefficient defined as $C_P = (p - p_S) / (\rho U^2 / 2)$, where p_S is the pressure at the position

of $\theta = 0^\circ$, decreases as the inclination angle increases and the Strouhal number and drag coefficient followed the IP for $\theta \leq 30^\circ$.

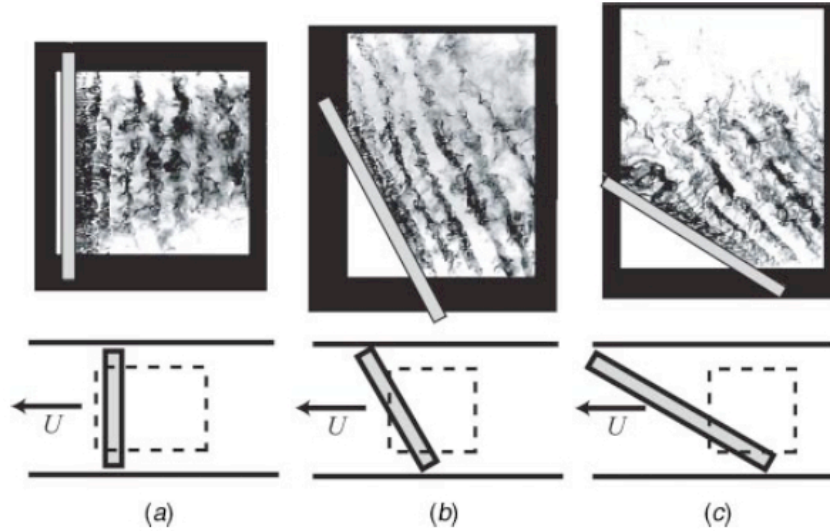


Figure 17. Vortex shedding behind an inclined cylinder towed in a tank for (a) 0° , (b) 30° and (c) 60° (Figure from Thakur et al., 2004).

The discrepancy of validity of IP between Lucor and Karniadakis (2003) and Zhao et al. (2009) is attributed to the use of varying aspect ratio (22 and 9.6 respectively). In order to avoid the discrepancy caused based on the aspect ratios, Willden and Guerbi (2010) performed DNS analysis on a fixed and forced vibrating cylinder with an aspect ratio of 50 for angles of inclination ranging from 0° to 80° . For stationary cylinders, they validated IP for the angles of inclination between 40° to 60° . The shedding angle for 60° inclined stationary cylinder was around 11° (similar to Lucor and Karniadakis, 2003) and for the cylinder inclined at 80° they observed shedding angle to be the same as the angle of inclination. From Figure 18, it can be seen that the flow variables decrease almost linearly with the decrease in angle of inclination. The ratio of normalized coefficients to the actual coefficients around unity implies the validity of IP in Figures 18d, e and f.

Willden and Guerbi (2010) also performed simulations for forced oscillating cylinders ($A/D = 0.3$) exposed to inclined flow and validated IP till 60° inclination angle.

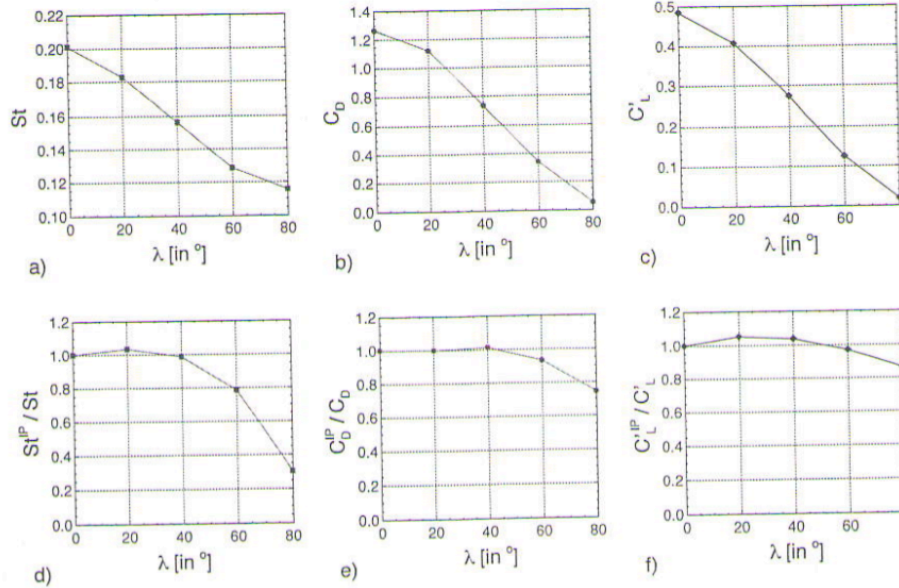


Figure 18. Influence of angle of Inclination on (a) Strouhal number, (b) Drag Coefficient, (c) Lift coefficient; (d), (e) and (f) the ratio of normalized coefficients after applying the IP to actual coefficients (Figure from Willden and Guerbi, 2010).

Yeo and Jones (2008) performed Detached Eddy Simulation (DES) to study the three-dimensional characteristics at very high Reynolds number (1.4×10^5) around an inclined cylinder ($\theta = 30^\circ$ and 45°). They pointed that the flow is highly three-dimensional with the vortex lines around the cylinder neither parallel nor linearly oblique to the cylinder axis. Similarly, Chen and Li (2009) performed Reynolds-Averaged Navier-Stokes (RANS) simulation to study the vortex-induced vibration in a 30° inclined Carbon Fiber Reinforced Polymer (CFRP) stay cable (taking into consideration the wind profile). They found a maximum cross-flow displacement of $0.189D$ at mid-span with remarkable fluctuation in the lift coefficient amplitude, which varies along the span of the cable. VIV of non-circular cross-sections like square cylinders, inclined to the flow were studied by Sheard et al. (2010).

2.3.1. Amplitude and frequency response of flexibly mounted inclined cylinders

Recently, Franzini et al. (2009) performed experiments on inclined cylinders with a low $m^*\zeta$ placed in a water tunnel in the Re range of 2,000-8,000, for angles of inclination of 0° , 20° and 45° . They used cylinders with an aspect ratio of 18 and 24 in order to check the influence of aspect ratio. Because of the similarity of results for both aspect ratios, the cylinder with an aspect ratio of 18 was chosen to compare the results with other inclined cylinders. To avoid three-dimensionality in flow, they had a small gap ($0.09D$) between the cylinder bottom end and the test section floor.

They measured the non-dimensional amplitude (A^*) at different reduced velocities (U^*) for different inclinations. It can be seen in Figure 19 that the peak amplitude decreases as the inclination increases from 0° to 20° but it is the same for 45° when compared to 20° . The commencement of the oscillations delays as the inclination increases. The peak amplitudes are very similar in the initial branch of oscillations and the maximum amplitudes for the vertical cylinder and the inclined cylinder are 0.8 and 0.65 respectively in the U^* range of 5-6.

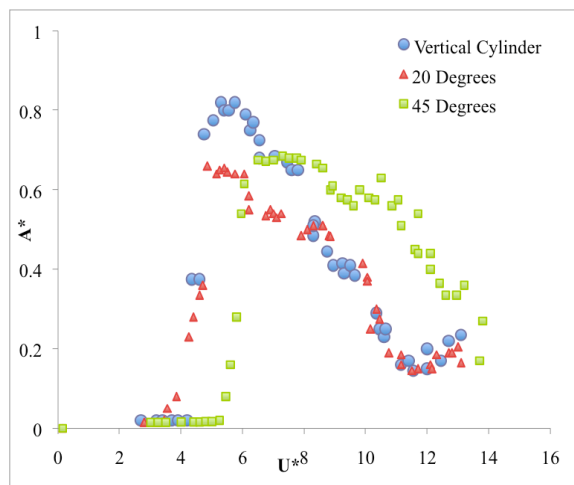


Figure 19. A^* plotted against U^* for 0° (\bullet), 20° (\blacktriangle) and 45° (\blacksquare) for $m^*\zeta = 0.0125$ (Reproduced from Franzini et al, 2009).

The frequency response as shown in Figure 20 indicates almost identical characteristics for the vertical and the inclined cylinder cases.

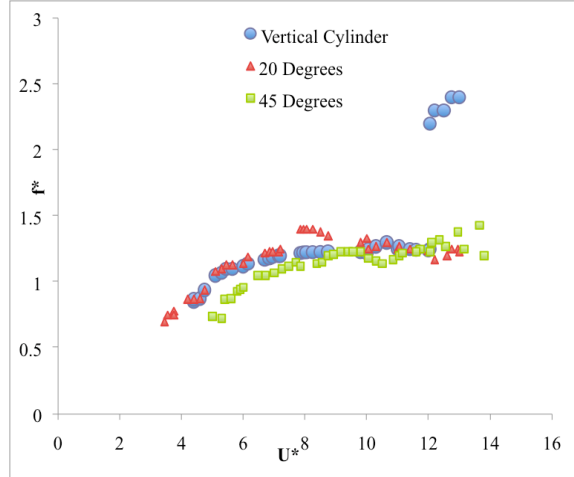


Figure 20. Non-dimensional frequency f^* versus the reduced velocity U^* for 0° (●), 20° (▲) and 45° (■) for $m^*\zeta = 0.0125$ (Reproduced from Franzini et al, 2009).

2.3.2. Fluid forces on flexibly mounted inclined cylinders

Franzini et al. (2009) measured the fluid forces acting on the cylinder and normalized it using $\frac{1}{2}\rho U^2 DL$ for the vertical cylinder. The r.m.s. lift coefficient and the drag coefficient had their maximum values of 2.2 and 2.3 respectively at the reduced velocity of $U^*= 4$ as shown in Figures 21 and 22. The lift and drag coefficients decrease as the inclination increases.

The variation of the wake flow in the cylinder's spanwise direction makes the lift coefficient vary along the cylinder length. Zhao et al. (2009) found that the difference between the total and sectional r.m.s. force coefficient is mainly because of the phase variation in the vortex shedding along the cylinder's spanwise direction. The total force coefficients are actually the results of the averaged sectional force coefficients. They found that the r.m.s. sectional drag coefficient was about twice of the r.m.s. total drag

coefficient and the r.m.s. sectional lift coefficient was also 7-10% larger than the r.m.s. total lift coefficient. In spite of the differences, the mean sectional drag coefficient was same as the mean total drag coefficient.

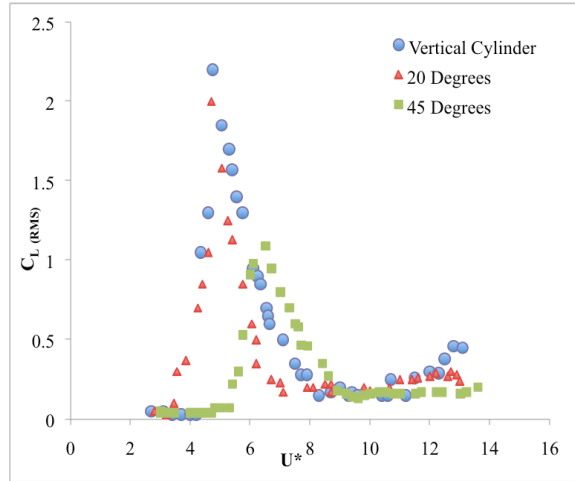


Figure 21. Lift coefficient $C_{L(RMS)}$ versus the reduced velocity U^* for 0° (\bullet), 20° (\blacktriangle) and 45° (\blacksquare) for $m^*\zeta = 0.0125$ (Reproduced from Franzini et al., 2009).

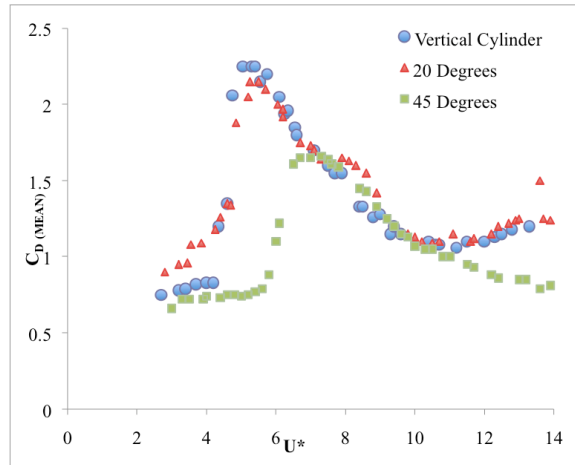


Figure 22. Drag coefficient $C_{D(MEAN)}$ versus the reduced velocity U^* for 0° (\bullet), 20° (\blacktriangle) and 45° (\blacksquare) for $m^*\zeta = 0.0125$ (Reproduced from Franzini et al., 2009).

2.3.3. Independence Principle (IP)

In order to check the validity of IP, Franzini et al. (2009) re-plotted the results in Figures 19-22 against the normal reduced velocity (U_n^*), which is given as:

$$U_n^* = \frac{U \cos \theta}{f_N D}. \quad (2.2)$$

Figure 23 shows that for all angles of inclination, the amplitude response is almost the same in the initial branch of oscillation ($U_n^* = 3.5-4.5$) and the maximum amplitudes occur in the same range of normal reduced velocity for all the cases. The frequency response (Figure 24) is almost identical for all the cases.

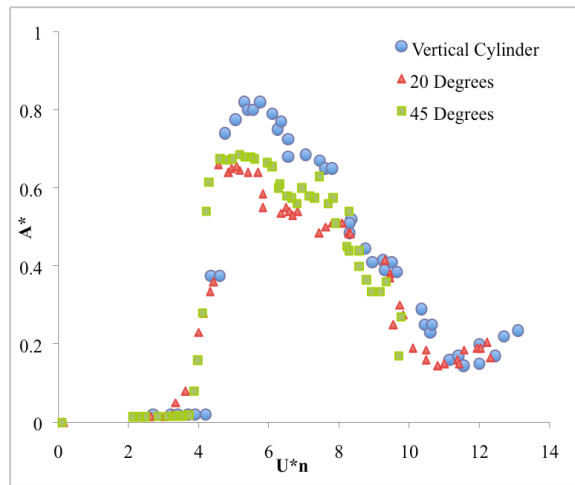


Figure 23. Non-dimensional A^* versus normal reduced velocity U_n^* after applying the IP for 0° (\bullet), 20° (\blacktriangle) and 45° (\blacksquare) for $m^*\zeta = 0.0125$ (Reproduced from Franzini et al., 2009).

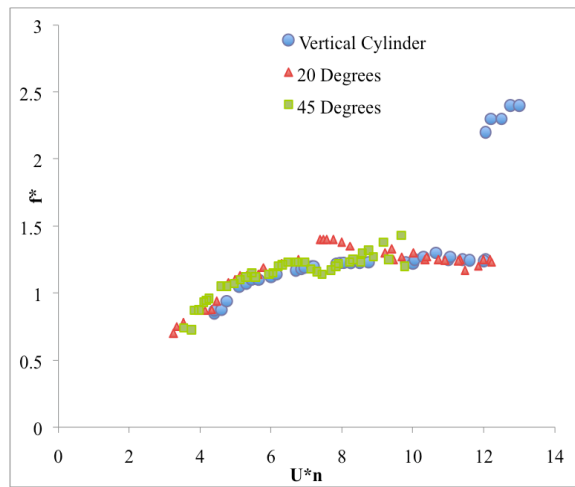


Figure 24. Non-dimensional frequency f^* versus the normal reduced velocity U_n^* after applying the IP for 0° (\bullet), 20° (\blacktriangle) and 45° (\blacksquare) for $m^*\zeta = 0.0125$ (Reproduced from Franzini et al., 2009).

The drag coefficient (Figure 25) and the lift coefficient (Figure 26) decrease as the angle of inclination increases, when plotted against the normal reduced velocity.

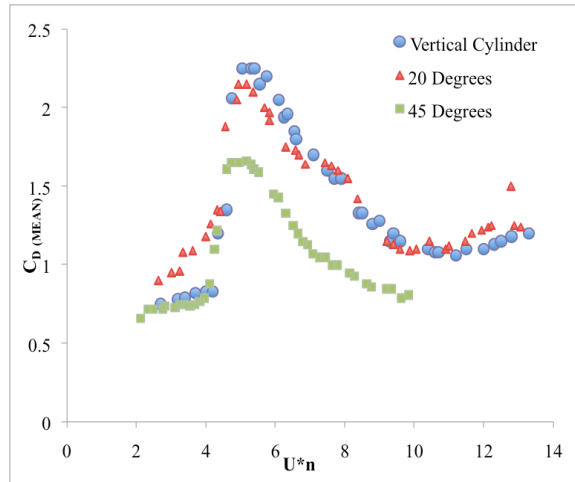


Figure 25. Drag coefficient $C_{D(MEAN)}$ versus the normal reduce velocity U^*_n after applying the IP for 0° (\bullet), 20° (\blacktriangle) and 45° (\blacksquare) for $m^*\zeta = 0.0125$ (Reproduced from Franzini et al., 2009).

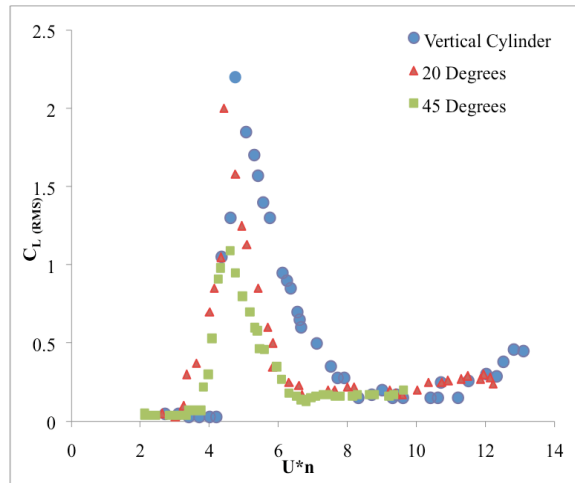


Figure 26. Lift coefficient $C_{L(RMS)}$ versus the normal reduced velocity U^*_n after applying the IP for 0° (\bullet), 20° (\blacktriangle) and 45° (\blacksquare) for $m^*\zeta = 0.0125$ (Reproduced from Franzini et al., 2009).

Table 2 summarizes various studies on inclined cylinder in flow.

Table 2. Enlisting the research work done on inclined cylinder

Author (year)	Fixed/ Moving Cylinder	IP Validity	Angle(s) of Inclination Discussed	Comments
Hanson (1966) (Experimental)	Moving	Yes	$\theta < 68^\circ$	Vortex shedding frequencies deviation is found at $\theta=70^\circ$ using Strouhal number (St).
Surry and Surry (1967) (Experimental)	Fixed	Yes	$40^\circ \leq \theta \leq 50^\circ$	IP was valid based on the St using the normal velocity component.
Van Atta (1968)	Fixed	Yes	$\theta \leq 35^\circ$	He validated IP based on the vortex shedding behind the cylinder. Vortex shedding was slower than predicted by IP beyond 35° .
Ramberg (1983) (Experimental)	Fixed/ Forced Oscillation	No (fixed) Yes (forced oscillation)	$\theta \leq 60^\circ$ (fixed) $\theta \leq 50^\circ$ (forced oscillation)	For stationary cylinder, vortex-shedding frequency is larger than IP and the shedding angle, vortex formation length, the base pressure and the wake width are all less than expected. For moving cylinder, because of the parallel shedding, St follows IP.
Kozakiewicz et al. (1995)	Fixed	Yes	$\theta < 55^\circ$	Based on the flow visualizations, streamlines were perpendicular to the cylinder axis till 55° . At 55° and 70° , the water particles moved along the cylinder axis rather than perpendicularly.
Lucor and Karniadakis (2003) (DNS)	Fixed/ Moving	No	$-60^\circ \geq \theta \geq -70^\circ$	The drag coefficient is larger than predicted by IP.
Zhao et al. (2009) (DNS)	Fixed	No	$\theta \leq 60^\circ$	The Strouhal number and mean drag coefficient followed IP for $\theta \leq 30^\circ$ whereas; the rms lift coefficient is smaller than IP.
Franzini et al. (2009) (Experimental)	Moving	Yes	$\theta \leq 45^\circ$	The lock-in region, after applying IP converged into the same range for all the Inclination.
Willden and Guerbi (2010) (DNS)	Fixed/ Forced Oscillation	Yes	$\theta \leq 40^\circ$ (Fixed) $\theta \leq 60^\circ$ (Forced Oscillation)	For stationary cylinder, Strouhal number follows IP at 40° and the critical angle is between 40° and 60° . For forced vibrating cylinder, parallel shedding is observed till 60° .

As discussed above, the majority of research conducted to study inclined cylinders in flow are for fixed cylinders and only few deal with the study of VIV of flexibly mounted inclined cylinder. Experimentally, the work of Franzini et al. (2009) provides an insight but it is restricted to small angles of inclination (0° , 20° and 45°). For higher angles of inclination, Lucor and Karniadakis (2003) using numerical simulation proves the invalidity of IP in the inclination range of $-60^\circ \geq \theta \geq 70^\circ$ based on the drag force. There are conflicting conclusions in terms of the critical angle of inclination for the validity of IP and many unanswered questions including:

1. What is the critical angle of inclination beyond which IP is not valid?
2. How does the cylinder's response change by varying system parameter such as the mass ratio?
3. Do we see any oscillation for large angle of inclination?
4. How will the flow pattern change with varying angles of inclination?

The present study aims to answer the above questions by conducting experiments in a water tunnel on a flexibly mounted rigid cylinders inclined to an angle of inclination up to 75° in the Reynolds number range of 500-4,000.

CHAPTER 3

EXPERIMENTAL SETUP AND RESULTS

3.1. Experimental Setup

The experiments were performed in a re-circulating water tunnel with a test section of $1.27\text{ m} \times 0.50\text{ m} \times 0.50\text{ m}$ with turbulence intensity of less than 1% RMS up to 0.3 m/s flow velocity. To reduce the damping in the system, two air bearings were mounted on rigid parallel shafts located atop the water tunnel test section, resulting in a one-degree-of-freedom system with oscillations in the cross-flow direction only (Figure 27).



Figure 27. Experimental Setup.

The natural frequency (f_N) and the structural damping of the system were measured by performing a decay test in air as shown in Figure 28. The structural damping coefficient (ζ) of the system is around 0.0045 and the mass ratio ($m^* = 4m/\pi\rho D^2L$) of the cylinder is approximately 6.5, leading to a mass-damping coefficient of $m^*\zeta = 0.029$ for all angles of inclination. The natural frequency of the system was 1.0 Hz. The mass of the system includes the mass of the cylinder and the moving objects such as the air bearings and the supporting plate for mounting the cylinder. Solid aluminum cylinders with a diameter (D) of 12.7 mm were machined to achieve the desired inclination such that for each cylinder, the lower end was cut parallel to the test section floor. Cylinders with $\theta = 0^\circ, 20^\circ, 45^\circ, 55^\circ, 65^\circ$ and 75° were tested. The immersed aspect ratio (L/D) of the cylinders was kept constant at approximately 29 for every angle of inclination.

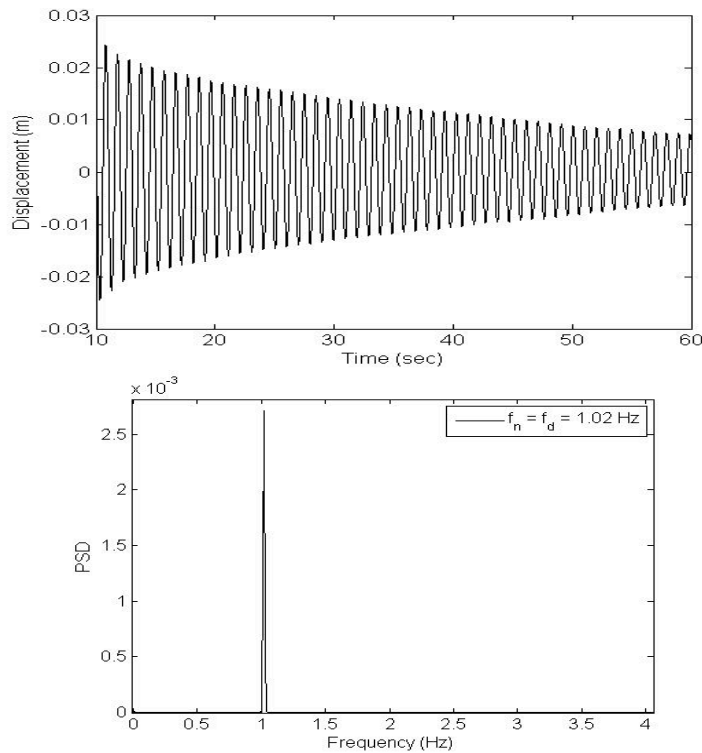


Figure 28. Decay test in air.

The end conditions of the cylinder play an important role in the observed VIV response as demonstrated by Morse et al. (2008). For a vertical or inclined cylinder partially submerged in water, the upper end of the cylinder is in contact with the free surface and the lower end is submerged in water. The free surface does not influence the parallel vortex shedding (Khalak and Williamson, 1996) but the lower end of the cylinder can induce three-dimensionality into the flow. The experiments here were performed on cylinders with an unattached streamlined end plate with a gap of 1 mm ($0.08D$). This gap size was chosen because for a normal-incidence cylinder, a gap size smaller than 15% of the cylinder diameter results in a behavior similar to a cylinder with an attached endplate – i.e., negligible three-dimensional effects due to the end condition – without increasing the added mass due to the attached endplate (Morse et al., 2008). Flow visualization was conducted on the endplate to make sure no major separation was resulted by the endplate’s leading edge. The displacement was measured using a Micro-Epsilon (ILD 1402-600) non-contacting laser sensor.

3.2. Experimental Results

For each inclination, the water level was held constant and the flow velocity was increased from zero in small steps. At each step the amplitude and frequency were calculated using the recorded displacement time series and the reduced velocity was calculated as $U^* = U/f_N D$.

3.2.1. VIV of vertical and inclined cylinders

One set of experiments was performed on a normal-incidence cylinder to have a base for comparison. These results were in agreement with those of Khalak and

Williamson (1999) in terms of the onset and width of the lock-in region as shown in Figure 29(a). The upper branch was not observed in our tests due to the difference in the mass-damping coefficient ($m^*\zeta$) compared with Khalak and Williamson's tests. Figure 29(b) shows the non-dimensional frequency ($f^* = f/f_N$, where f is the cylinder's oscillating frequency) plotted against U^* . As the flow velocity increases, the oscillating frequency (f) approaches the natural frequency (f_N) of the system and the cylinder starts oscillating in the crossflow direction.

In order to validate the IP, five sets of experiments were performed on cylinders with various angles of inclination up to 75° . Figure 30 shows the amplitude and frequency response for a 20° -inclined cylinder compared with the results from Franzini et al. (2009). The onset of lock-in region ($\approx U^* = 4$), the width of lock-in region (despite a slight difference at the end of the lock-in region) and the maximum amplitude ($A^* = 0.65$) are similar to the case of a vertical cylinder, which was predictable for such a small increase in the angle of inclination. The maximum amplitude is observed at around $U^* = 5$. It is also interesting to note that, despite the difference in $m^*\zeta$ and m^* compared to Franzini et al. (2009), the response amplitude in the current experiments is similar to their results. The absence of the upper branch in their case is in agreement with the current results. Higher f^* was observed in the results of Franzini et al. because of smaller cylinder mass ratio ($m^* = 2.5$). Similar frequency response for vertical cylinder with small mass ratio ($m^* = 2.4$) was also observed by Khalak and Williamson (1997b) with damping similar to current experiment ($\zeta = 0.45\%$).

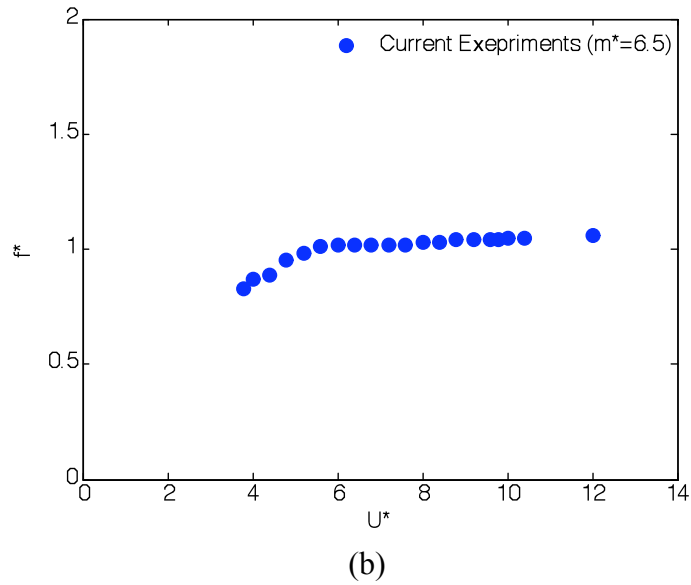
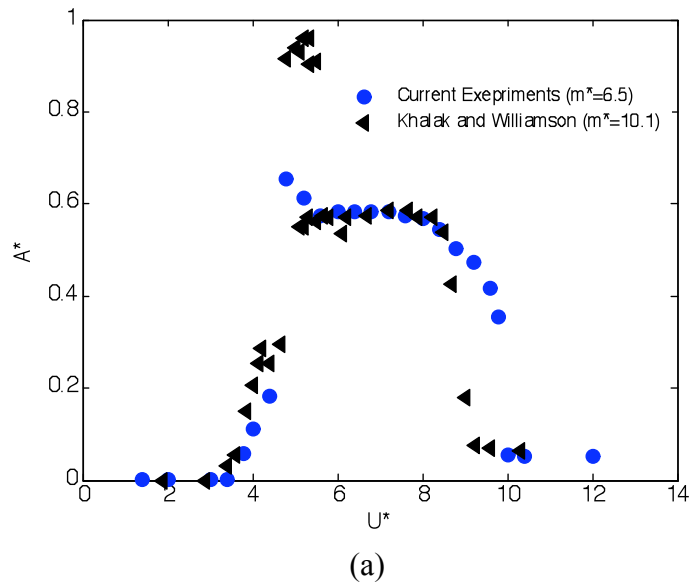
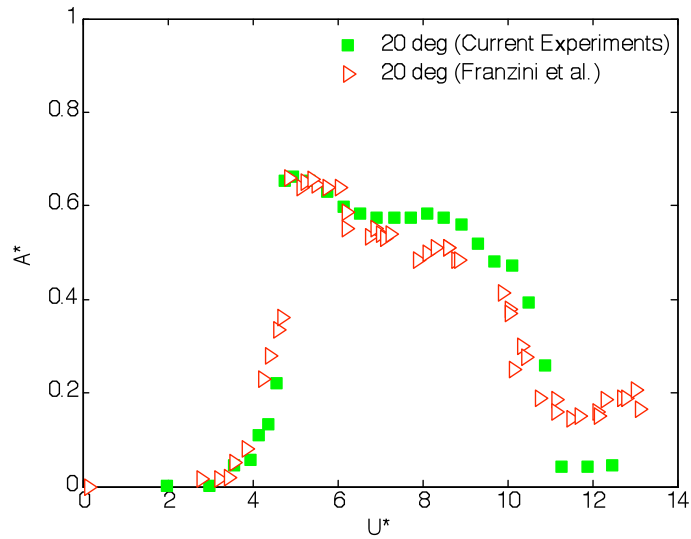
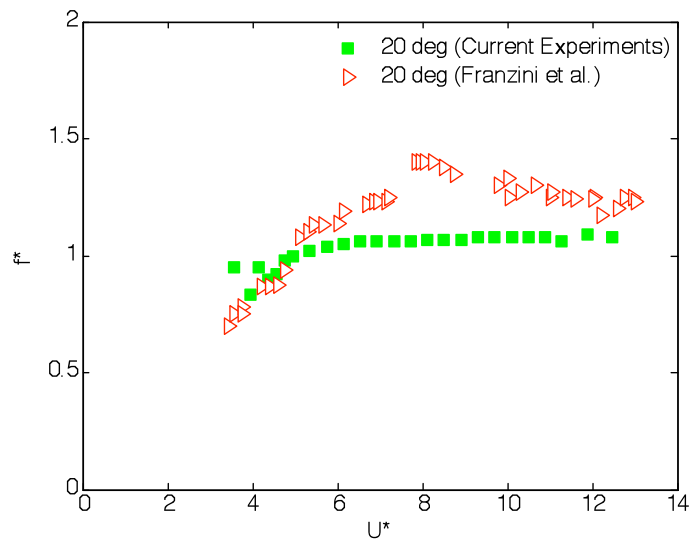


Figure 29. (a) Comparison of the results of the present experiments for a normal incidence cylinder ($m^*\zeta = 0.029$) with 1 mm gap ($0.08D$) with Khalak & Williamson's (1999) results ($m^*\zeta = 0.013$); (b) Frequency response for a normal-incidence cylinder ($m^*\zeta = 0.029$).



(a)



(b)

Figure 30. (a) Amplitude and (b) frequency response for a 20°-inclined cylinder with 1 mm gap (0.08D), based on the current experiments ($m^*\xi = 0.029$) and Franzini et al. (2009) ($m^*\xi = 0.0125$).

Figure 30 shows the amplitude and frequency response for a 20°-inclined cylinder compared with the results from Franzini et al. (2009). The onset of lock-in region ($\approx U^* = 4$), the width of lock-in region (despite a slight difference at the end of the lock-in region)

and the maximum amplitude ($A^*= 0.65$) are similar to the case of a vertical cylinder, which was predictable for such a small increase in the angle of inclination. The maximum amplitude is observed at around $U^*= 5$. It is also interesting to note that, despite the difference in $m^*\xi$ and m^* compared to Franzini et al. (2009), the response amplitude in the current experiments is similar to their results. The absence of the upper branch in their case is in agreement with the current results. Higher f^* was observed in the results of Franzini et al. because of smaller cylinder mass ratio ($m^*= 2.5$). Similar frequency response for vertical cylinder with small mass ratio ($m^*= 2.4$) was also observed by Khalak and Williamson (1997b) with damping similar to current experiment ($\xi = 0.45\%$).

The 45° -inclined cylinder's response is shown in Figure 31. The lock-in region delays to start at $U^*= 5.5$ compared to $U^*= 4$ in the case of a vertical cylinder. The maximum amplitude remains the same for the 45° -inclined, 20° -inclined and vertical cylinder. Non-dimensional frequency is around $f^*= 1$ almost throughout the lock-in range of $5 < U^* < 14$. The onset of the lock-in region and the maximum amplitude are similar to the results of Franzini et al. (2009).

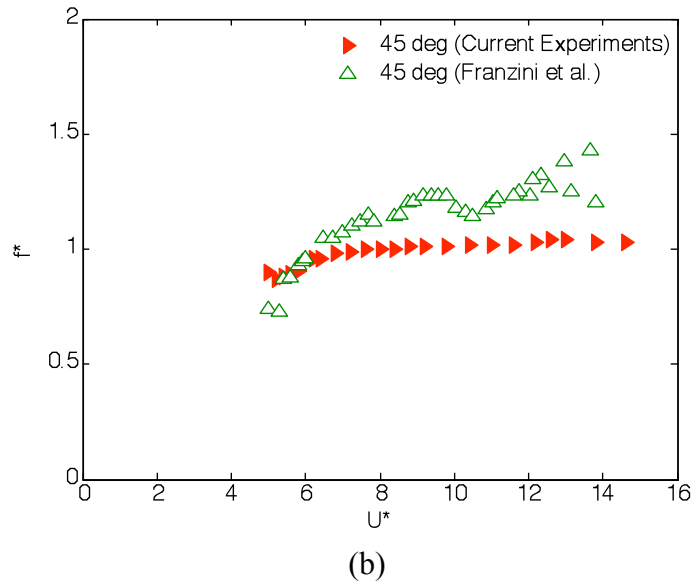
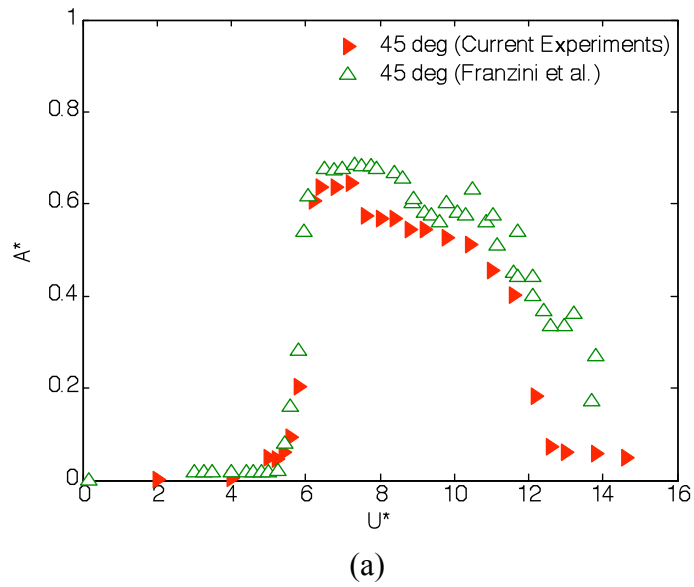
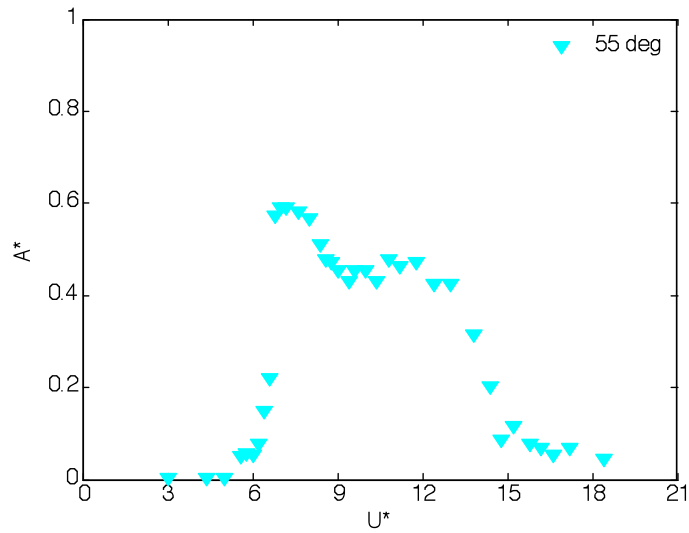
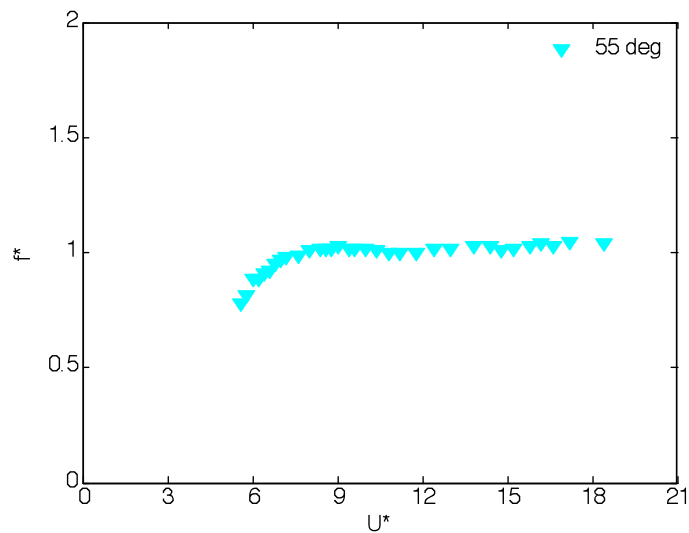


Figure 31. (a) Amplitude and (b) frequency response for a 45°-inclined cylinder with a 1 mm gap ($0.08D$), based on the current experiments ($m^*\xi = 0.029$) and Franzini et al. (2009) ($m^*\xi = 0.0125$).



(a)



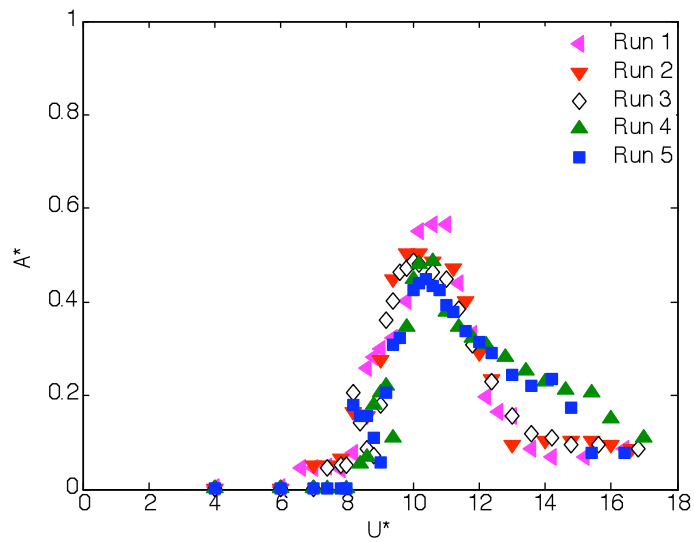
(b)

Figure 32. (a) Amplitude and (b) frequency response for a 55°-inclined cylinder with 1 mm gap (0.08*D*).

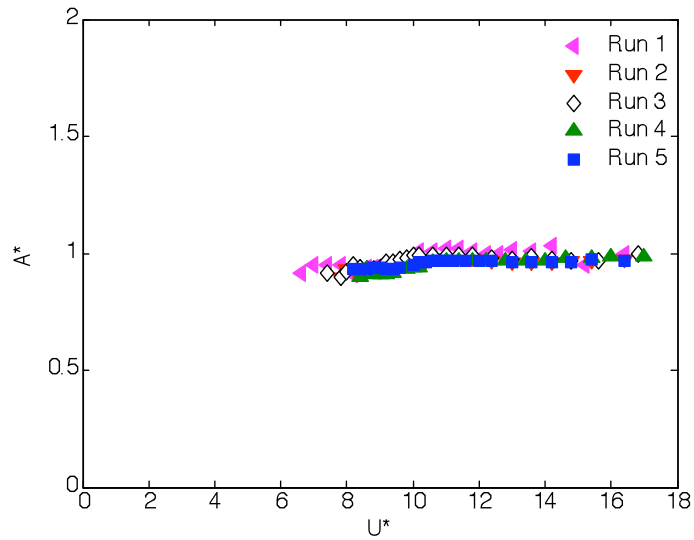
Figure 32 shows the amplitude and frequency response for $\theta = 55^\circ$ tested in the current experiments. The onset of lock-in region delays compared to smaller angles of inclination and the peak amplitude is decreased. Figures 33 and 34 show the amplitude and frequency for 65° and 75°-inclined cylinders. The width of the lock-in region

decreases as seen for both the angles when compared to 55°-inclined cylinder, indicating the possible dominant effect of axial component of flow velocity. The peak amplitude also decreases from 0.57 to 0.38 for 65° and 75° respectively. Various runs for 65°-inclined cylinder show the good repeatability of the experiments. The oscillating frequencies for all the cylinders remain close to the natural frequency of the system.

The amplitude and frequency response for all the angles of inclination are plotted in Figure 35. Based on this figure, it is true that “the lock-in range shrinks with increasing yaw angle but this will not necessarily diminish the magnitude of the self-excited response, rather it will simply delay its onset or hasten its completion a small amount for increasing flow speed” (Ramberg, 1983).

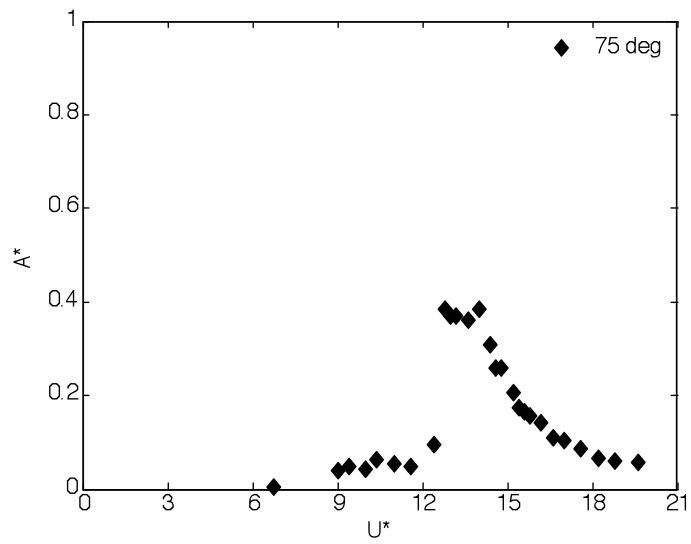


(a)

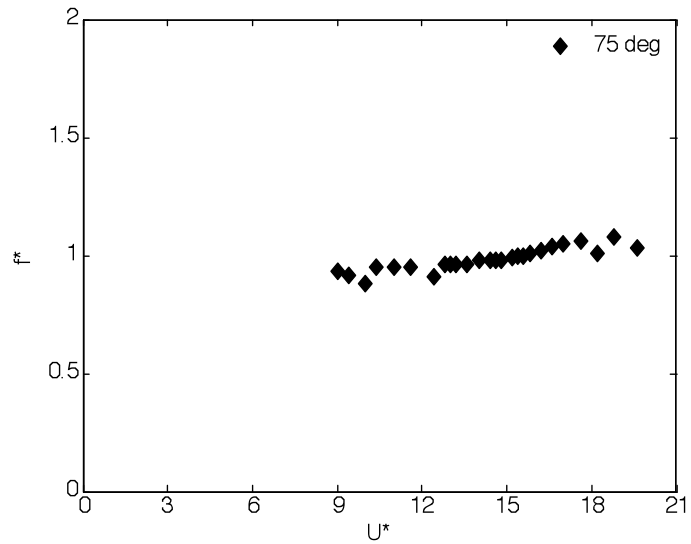


(b)

Figure 33. Various runs showing the (a) amplitude and (b) frequency response for a 65° -inclined cylinder with 1 mm gap ($0.08D$).

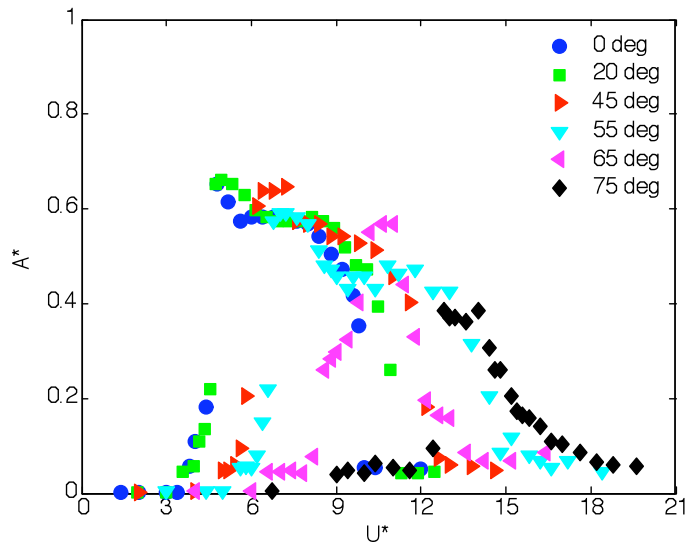


(a)

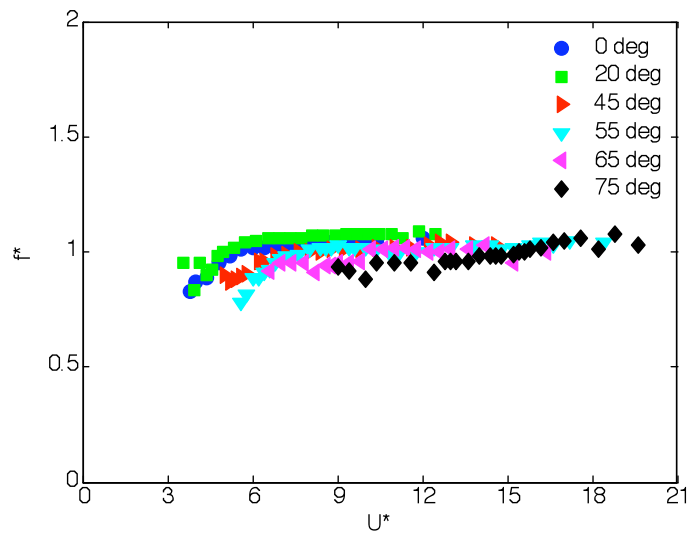


(b)

Figure 34. (a) Amplitude and (b) frequency response for a 75° -inclined cylinder with 1 mm gap ($0.08D$).



(a)



(b)

Figure 35. (a) Amplitude and (b) frequency response for all the angles of inclination with 1 mm gap ($0.08D$) and $m^*\zeta=0.029$.

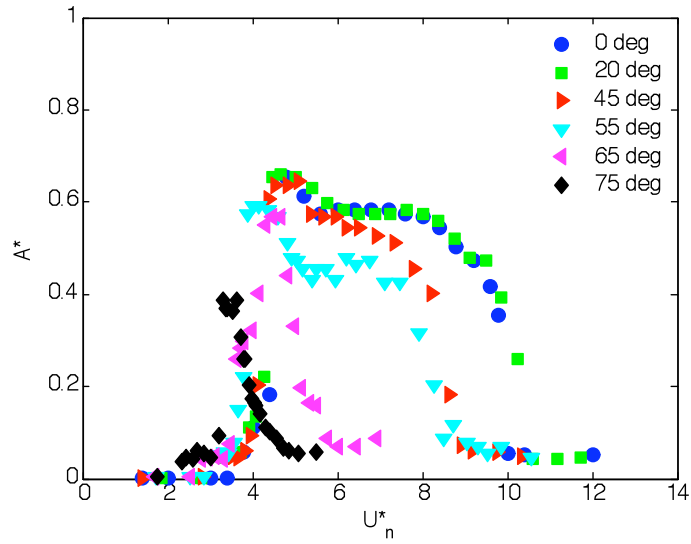
In order to validate the IP, the amplitude and frequency response were plotted against the normalized reduced velocity ($U_n^* = U^* \cos \theta$) in Figure 36. The lock-in region begins at $U_n^* \approx 4$ and the maximum amplitude is almost the same for all of these inclinations. The width of the lock in range remains the same for 0° and 20° , it decrease slightly for 45° and 55° , and there is a dramatic decrease in its width for 65° and 75° . For these last two angles of inclination, the lock in range changes its pattern and the relative wide plateau of the large amplitude oscillations observed for the lower angles of inclination disappears and instead the large-amplitude oscillation occurs over a very short range of normalized reduced velocities. The maximum amplitude for all inclinations, except 75° , lies in the U_n^* range of 4–6, in agreement with Ramberg (1983) and Lucor and Karniadakis (2003). The maximum amplitude is almost similar for 20° and 45° (also observed by Franzini et al., 2009) but it decreases as the angle of inclination decreases

Table 3. Peak amplitudes for different angles of inclination

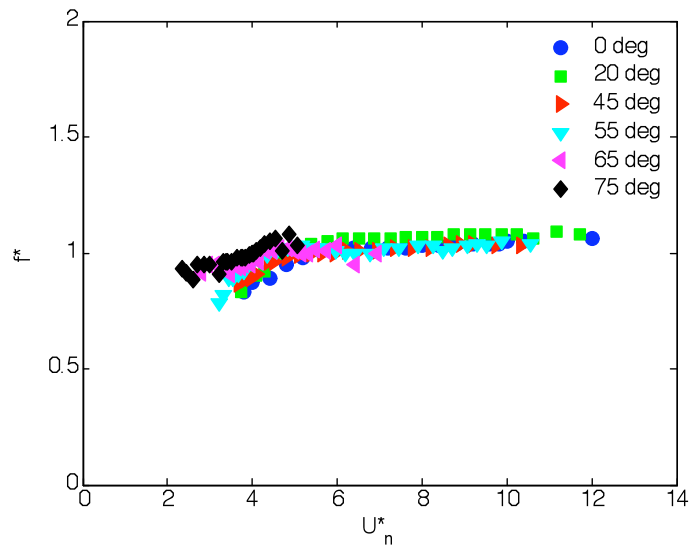
Angle of Inclination (θ)	Non-Dimensional Peak Amplitude (A^*)
0°	0.64
20°	0.65
45°	0.64
55°	0.59
65°	0.57
75°	0.38

from 55° to 75° . Lucor and Karniadakis (2003) observed decrease in the maximum amplitude A^* from 0.63 to 0.52 for -60° and -70° -inclined cylinder respectively. In the present case, the peak amplitude A^* decreases from 0.57 to 0.38 for 65° and 75° angle of

inclination respectively. The peak amplitudes for various inclinations are given in Table 3.



(a)



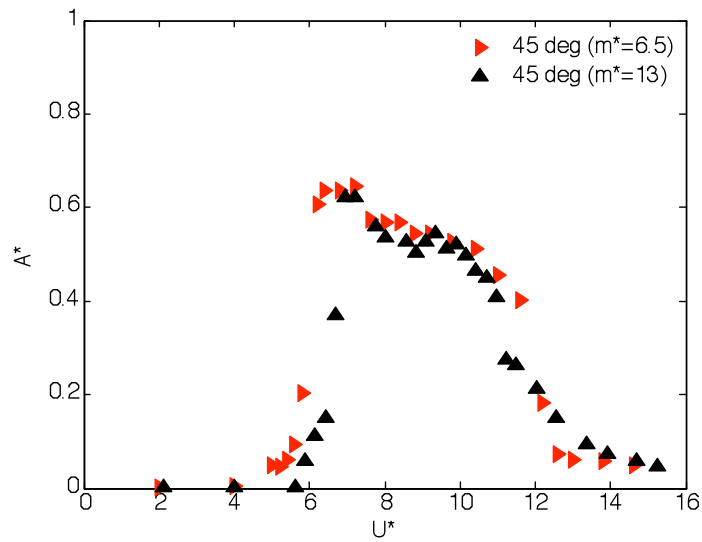
(b)

Figure 36. (a) Amplitude and (b) frequency response for all the angle of inclination after applying the Independence Principle ($U_n^* = U^* \cos \theta$) with 1 mm gap ($0.08D$) and $m^* \zeta = 0.029$.

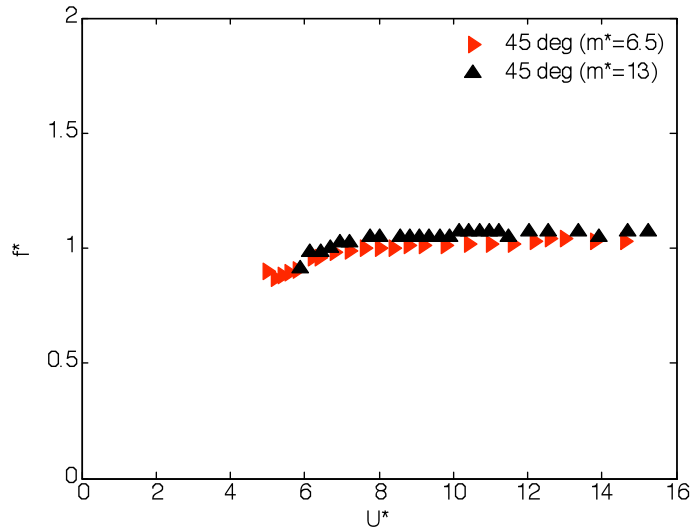
3.2.2. Effect of the mass ratio on VIV of inclined cylinders

Another series of experiments were performed on 45° and 65°-inclined cylinders with a different mass ratio $m^*= 13$ (instead of $m^*= 6.5$) and with the same damping coefficient ($\zeta= 0.0045$) leading to $m^*\zeta= 0.0585$. The mass ratio was increased by putting dummy weights on top of the plate holding the test cylinder. Because of the increase in mass, the natural frequency f_N of the system reduced to 0.75 Hz from 1.0 Hz. The end plates were used to maintain the 1 mm gap ($0.08D$) similar to the earlier experiments.

The higher m^* does not seem to have any significant impact on the amplitude and frequency response of 45°-inclined cylinder as shown in Figure 37. The lock-in range and the maximum amplitude are similar to the case with $m^*= 6.5$. Figure 38 shows the effect of increasing mass ratio on the 65°-inclined cylinder. The width of the lock-in region increases till $U^*= 16$ for the system with a larger mass ratio. The effect of doubling the mass ratio does not have any significant effect on the validity of IP. As shown in Figure 39, the width of the lock in range decreases dramatically as the angle of inclination changes from 45° to 65°, in agreement with the results of the smaller added mass discussed previously. It ought to be mentioned that although the case of $m^*=13$ is considered a relatively higher mass ratio case, it does not represent a high-mass ratio case as could be obtained in tests conducted in air flow, instead of water flow.

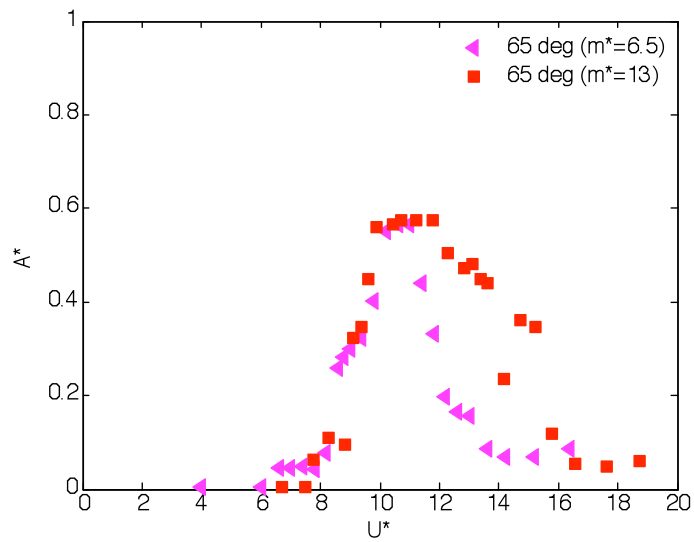


(a)

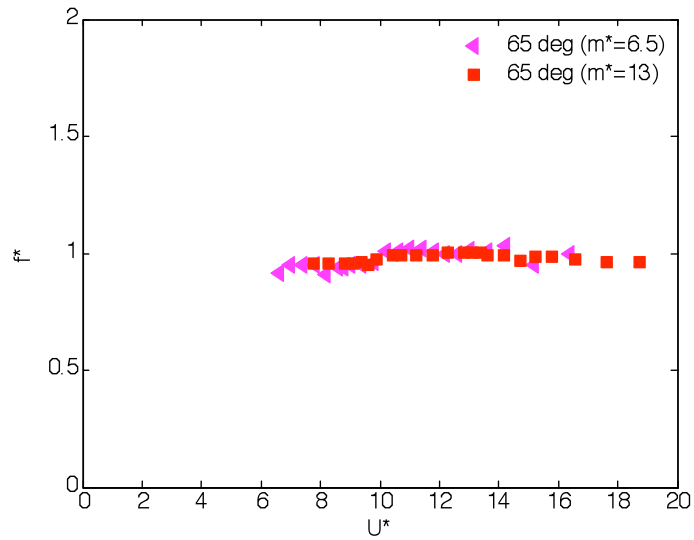


(b)

Figure 37. Comparison of (a) amplitude and (b) frequency response for 45°-inclined cylinder with $m^* = 6.5$ ($m^*\xi = 0.029$) and $m^* = 13$ ($m^*\xi = 0.0585$) with 1 mm gap ($0.08D$).

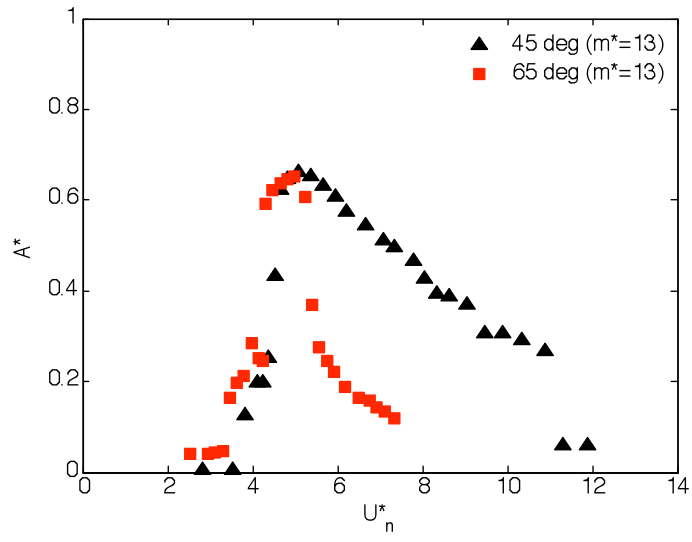


(a)

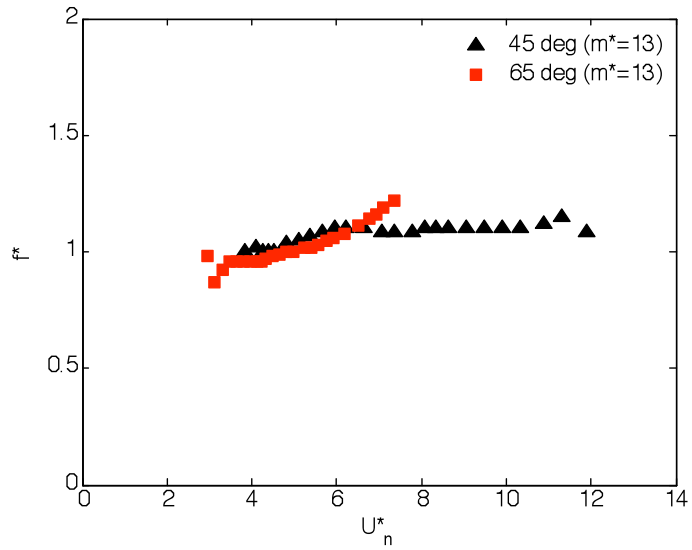


(b)

Figure 38. Comparison of (a) amplitude and (b) frequency response for 65°-inclined cylinder with $m^*= 6.5$ ($m^*\zeta= 0.029$) and $m^*= 13$ ($m^*\zeta= 0.0585$) with 1 mm gap ($0.08D$).



(a)



(b)

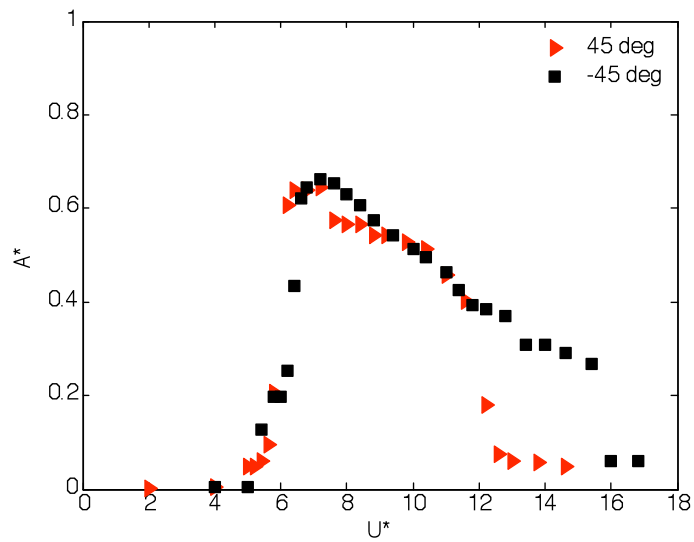
Figure 39. (a) Amplitude and (b) frequency response after applying IP to 45° and 65°-inclined cylinder with $m^* = 13$ ($m^* \zeta = 0.0585$).

3.2.3. Effect of positive and negative angles on VIV of inclined cylinders

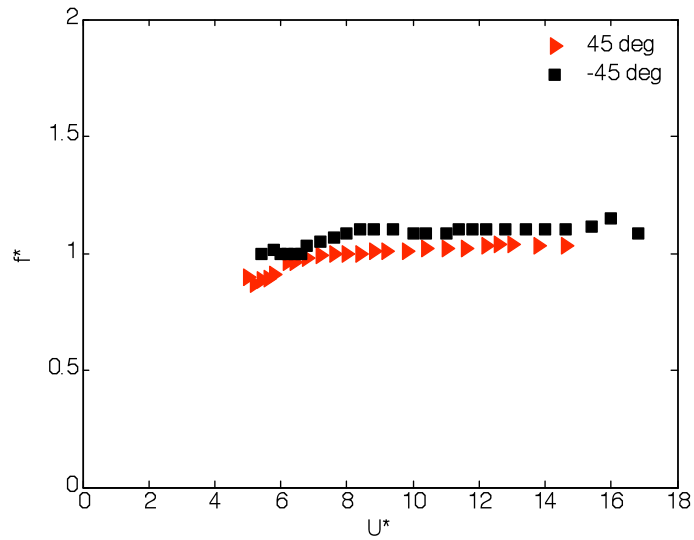
King (1977) showed that the inclined cylinders response was identical for positive and negative angles of inclination ($-45^\circ < \theta < 45^\circ$) in his experiments. We investigate this behavior for $\pm 45^\circ$ and $\pm 65^\circ$ -inclined cylinders.

Figure 40 shows the amplitude and frequency response for $\pm 45^\circ$ -inclined cylinder. The response is similar in terms of the onset of lock-in and the maximum amplitude but the width of the lock-in region increases for -45° -inclined cylinder. This difference could be due to the end condition effects. The oncoming flow first approaches the bottom end of the cylinder leading to axial flow moving up the cylinder, as opposed to down in the previous case.

The effect of negative angle of inclination on 65° -inclined cylinder is also similar to 45° -inclined cylinder as shown in Figure 41. The frequency response for -65° -inclined cylinder is close to unity but it increases at the end of the lock-in region. The maximum amplitude and the width of the lock-in region increase for the -65° -inclined cylinder. The maximum cylinder response is around $A^* = 0.64$ very close to Lucor and Karniadakis (2003) results. They had performed numerical simulation on a -60° -inclined cylinder with $m^*\zeta = 0.003$ ($m^* = 2$) and observed a maximum amplitude of $A^* = 0.63$. An important point to note is that even though similar maximum amplitudes are observed in both cases, their $m^*\zeta$ was an order of magnitude smaller than the current experiments. As shown in Figure 42, the negative angle of inclination does not affect the validity of IP compared to the positive angles of inclination shown in Figure 36.



(a)



(b)

Figure 40. Comparison of (a) amplitude and (b) frequency response for $\pm 45^\circ$ -inclined cylinder with 1 mm gap ($0.08D$) and $m^*\xi = 0.029$.

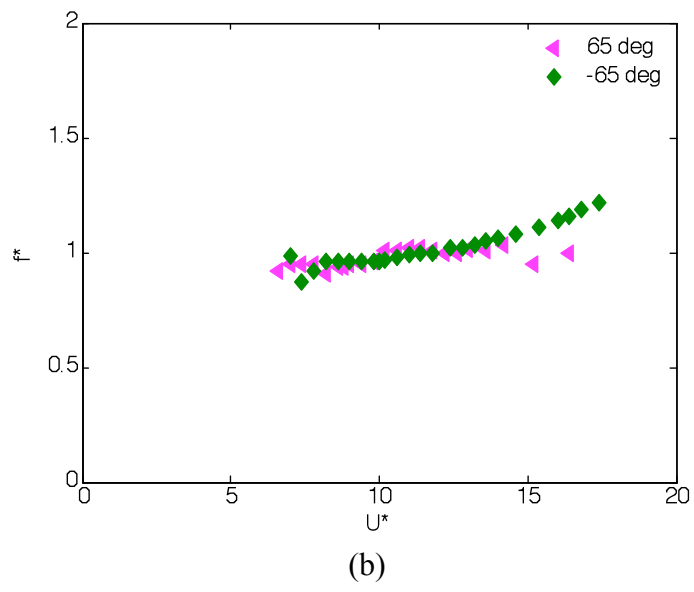
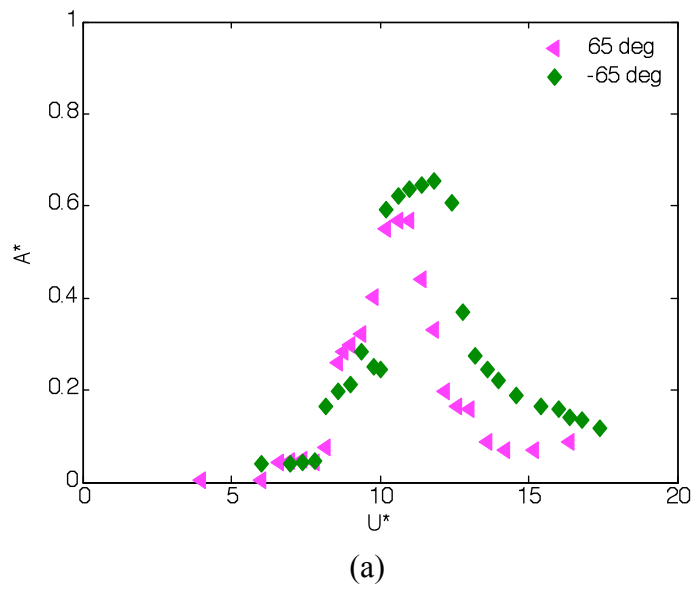
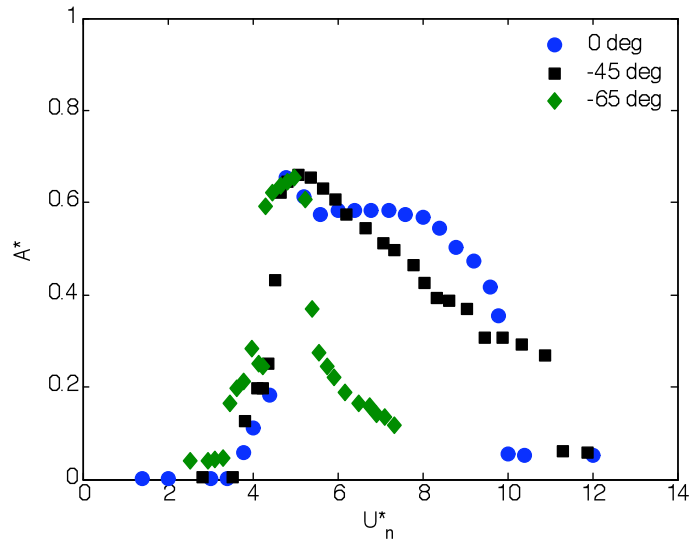
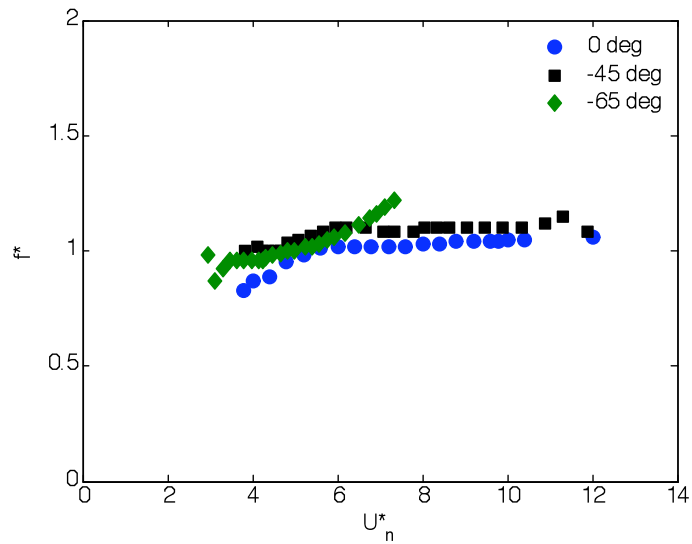


Figure 41. Comparison of (a) amplitude and (b) frequency response for $\pm 65^\circ$ -inclined cylinder with 1 mm gap ($0.08D$) and $m^*\zeta = 0.029$.



(a)



(b)

Figure 42. (a) Amplitude and (b) frequency response after applying IP to -45° and -65° -inclined cylinder with $m^* = 6.5$ ($m^*\xi = 0.029$).

3.2.4. Flow Visualization

In order for IP to be valid, the inclined cylinder must behave similarly to vertical cylinder in terms of the onset of lock-in, its width and the magnitude of VIV. Another important criterion is that the Von Karman vortex street should be parallel to the cylinder's axis, which will be discussed in this section.

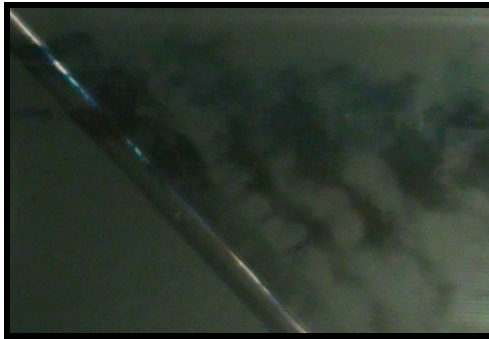
The flow visualization was conducted using colored dye to observe the Von Karman vortex street in the wake of the oscillating cylinder with angles of inclination of $\theta = 0^\circ$, 45° and 65° . Figure 43(a) shows the parallel vortex shedding in the wake of the vertical cylinder as expected. The shedding pattern is of the type 2S. The physical importance of parallel shedding is directly related to the spanwise coherence of vortex shedding which in turn reflects the spanwise correlation of fluctuating lift force (Ramberg, 1983).

In the wake of the 45° -inclined cylinder as shown in Figure 43(b), the vortices are also shed parallel to the cylinder axis. Ramberg (1983) performed flow visualization on freely moving cylinder and observed parallel vortex shedding till $\theta = 50^\circ$. Here, parallel vortex shedding is observed in the wake of the 65° -inclined cylinder as shown in Figure 43(c), in agreement with Lucor and Karniadakis (2003), who observed parallel vortex shedding for -60° and -70° -inclined cylinder in their numerical simulation.

The parallel shedding is observed even in cases with large angles of inclination, which suggests that the shedding is forced to be parallel by the movement of the cylinder.



(a) 0° , $U^* = 4.4$



(b) 45° , $U^*_n = 4.4$



(c) 65° , $U^*_n = 4.3$

Figure 43. Flow visualization in the wake of (a) vertical cylinder, (b) 45° -inclined cylinder and (c) 65° -inclined cylinder. Flow is from left to right.

CHAPTER 4

CONCLUSIONS

A series of experiments were conducted to study vortex-induced vibrations of flexibly mounted rigid inclined cylinders with one degree of freedom – transverse to the oncoming flow. Angles of inclination from 0 to 75° in the subcritical Re range of 500-4000 were considered. For $m^*\xi = 0.029$, the upper branch was absent for the vertical cylinder, in agreement with previous results. The onset of lock-in region delayed as the angle of inclination was increased when plotted against U^* . The maximum amplitude ($A^* = 0.66$) for 20° and 45°-inclined cylinder were in agreement with Franzini et al. (2009) despite the difference in mass-damping factor ($m^*\xi = 0.0125$ – Franzini et al., 2009). For $\theta = 55^\circ, 65^\circ$ and 75° , the maximum A^* decreased to 0.59, 0.57 and 0.39 respectively. After applying the Independence Principle (IP), the width of the lock-in region decreased with increasing angle of inclination, and for 75°-inclined cylinder it was in the U_n^* range of 3-5. The frequency response was close to unity for all the angle of inclination. It turned out that the IP is not valid for angles of inclination larger than 55°, as the width and the pattern of the lock in region changed dramatically for larger angles.

Experiments were also performed to study the effect of mass ratio (m^*) on the results. Cases of 45° and 65°-inclined cylinder were considered with the same damping coefficient as previous runs ($\xi = 0.0045$). The mass ratio was increased from 6.5 to 13 leading to $m^*\xi = 0.058$. The change in mass ratio did not have any significant effect on the 45°-inclined cylinder, but in the case of 65°-inclined cylinder the lock-in region increased. The IP was not valid for 65°.

Tests were also conducted on 45° and 65°-inclined cylinder to see the difference in cylinders response with a negative angle of inclination. The width of the lock-in region increased for both angles compared to the positive angles, but the onset of lock-in remained the same. No effect was seen on the maximum amplitude of the 45°-inclined cylinder but for $\theta= 65^\circ$, the maximum amplitude increased marginally from 0.57 to 0.65.

Finally, flow visualization was performed using colored dye on vertical cylinder, 45° and 65°-inclined cylinder. Parallel vortex shedding was observed for all three cases in agreement with Ramberg (1983) and Lucor and Karniadakis (2003).

BIBLIOGRAPHY

- [1] Bearman, P. W., Brankovic, M., 2006. Measurements of transverse forces on circular cylinders undergoing vortex-induced vibration. *Journal of Fluids and Structures* 22, 829-836.
- [2] Lucor D., Karniadakis G. E. M., 2003. Effects of oblique inflow in VIV. *Flow, Turbulence and Combustion* 71, 375-389.
- [3] El Baroudi, M. Y., 1960. Measurement of two point correlations of velocity near a circular cylinder shedding a Karman vortex street. University of Toronto, UTIAS, TN31.
- [4] Feng, C. C., 1968. The measurement of vortex-induced effects in flow past a stationary and oscillating circular and D-section cylinders. Masters thesis, University of British Columbia, Vancouver, B.C Canada.
- [5] Franzini, G. R., Fajarra, A. L. C., Meneghini, J. R., Korkischko, I., Franciss, R., 2009. Experimental investigation of Vortex Induced Vibration on rigid, smooth and inclined cylinders. *Journal of Fluids and Structures* 25, 742-750.
- [6] Gerrard, J. H., 1966. The mechanics of the formation region of vortices behind bluff bodies. *Journal of Fluid Mechanics* 25, 401-413.
- [7] Gerlach, C. R., Dodge, F. T., 1970. An engineering approach to tube flow-induced vibrations. *Proc. Conference on Flow-Induced Vibrations in Reactor System Components*. 205-225.
- [8] Govardhan, R., Williamson, C. H. K., 2000. Modes of vortex formation and frequency response of a freely vibrating cylinder. *Journal of Fluid Mechanics* 420, 85-130.
- [9] Griffin, O. M. & Ramberg, S. E., 1974. The vortex street wakes of vibrating cylinders. *Journal of Fluid Mechanics* 66, 553-576.
- [10] Griffin, O. M., 1980. Vortex-excited crossflow vibrations of a single cylindrical tube, *ASME Journal of Pressure Vessel Technology* 102, 158-166.
- [11] Hanson, A. R., 1966. Vortex-shedding from yawed cylinders. *AIAA Journal* 4(4), 738-740.
- [12] Humphreys, J. S., 1960. On a circular cylinder in a steady wind at transition Reynolds number. *Journal of Fluid Mechanics* 9, 603-612.
- [13] Khalak, A., Williamson, C. H. K., 1996. Dynamics of a hydro elastic cylinder with very low mass and damping. *Journal of Fluids and Structures* 10, 455-472.

- [14] Khalak, A., Williamson, C. H. K., 1997a. Investigation of relative effects of mass and damping in vortex-induced vibration of a circular cylinder. *Journal of Wind Engineering and Industrial Aerodynamics* 69-71, 341-350.
- [15] Khalak, A., Williamson, C. H. K., 1997b. Fluid forces and dynamics of a hydro elastic structure with very low mass and damping, *Journal of Fluids and Structures* 11, 973-982.
- [16] Khalak, A., Williamson, C. H. K., 1999. Motions, forces and mode transitions in vortex-induced vibrations at low mass damping, *Journal of Fluids and Structures* 13, 813–851.
- [17] King, R., 1977. Vortex excited oscillations of yawed circular cylinders. *ASME Journal of Fluids Engineering*, 495–502.
- [18] Kozakiewicz, A., Fredsøe, J. and Sumer, B., 1995. Forces on Pipelines in Oblique Attack: *Steady Current and Waves*, Vol. II. The Hague, Netherlands, 174–183.
- [19] Morse, T. L., Govardhan, R., Williamson, C. H. K., 2008. The effect of end conditions on the vortex-induced vibration of cylinders, *Journal of Fluids and Structures* 24, 1227- 1239.
- [20] Ramberg, S., 1983. The effects of yaw and finite length upon vortex wakes of stationary and vibrating circular cylinders. *Journal of Fluid Mechanics* 128, 81–107.
- [21] King R., July 1977. A review of vortex shedding research and its application. *Ocean Engineering Volume 4*, Issue 3, 141-171.
- [22] Schewe, G., 1983. On the force fluctuations acting on a circular cylinder in cross-flow from subcritical up to transcritical Reynolds numbers. *Journal of Fluid Mechanics* 133, 265–285.
- [23] Sheard, G., Fouras, A., Hourigan, K., June, 2010. PIV measurement of a subharmonic “Mode C” three-dimensional instability behind inclined square cylinders. *Proceedings of the IUTAM Symposium on Bluff Body Wakes and Vortex-Induced Vibrations*, 253-256.
- [24] Stansby, P. K., 1974. Effects of end plates on base pressure coefficient of a circular cylinder. *Aeronautical Journal* 78, 36–37.
- [25] Surry, J. and Surry, D., 1967. The effect of inclination on the Strouhal number and other wake properties of circular cylinders at subcritical Reynolds numbers. Technical Report, UTIAS Technical note No. 116, Institute for Aerospace Studies, University of Toronto.

- [26] Thakur, A., Liu, X., Marshall, J. S., 2004. Wake flow of single and multiple yawed cylinders. *ASME Journal of Fluids Engineering* 126, 861–870.
- [27] Van Atta, C. W., 1968. Experiments on vortex shedding from yawed circular cylinders. *AIAA Journal* 6, 931–933.
- [28] Vlachos, P. P., Tellionis, D. P., 2008. The effect of free surface on the vortex shedding from inclined circular cylinders. *ASME Journal of Fluids Engineering* 130, 021103.1–021103.9.
- [29] Vikestad, K., Vandiver, J. K. and Larsen, C. M., 2000. Added mass and oscillation frequency for a circular cylinder subjected to vortex-induced vibrations and external disturbance. *Journal of Fluid and Structures* 14, 1071-1088.
- [30] Wenli Chen and Hui Li, 2009. Vortex – Induced vibration of stay cable under profile velocity using CFD numerical simulation method. *Frontiers of Architecture and Civil Engineering in China*, Volume3, Number 4, 357-363.
- [31] Willden, R. H. J., Guerbi, M., 2010. Vortex dynamics of stationary and oscillating cylinders in yawed flow. *Proceedings of the 6th symposium on bluff body vortex induced vibrations (BBVIV-6)*, Capri, Italy, June 2010.
- [32] Yeo, D., Jones, N., 2008. Investigation on 3-D characteristics of flow around a yawed and inclined circular cylinder. *Journal of Wind Engineering and Industrial Aerodynamics* 96, 1947-1960.
- [33] Yeo, D., Jones, N. 2008. Effects of spanwise boundary conditions and aspect ratios on flow around a yawed and inclined circular cylinder. *The 4th International Conference on Advances in Wind and Structures (AWAS'08)*.
- [33] Zdravkovich, M. M., 2003. *Flow Around Circular Cylinders*, vol. 2: Applications. Oxford University Press.
- [35] Zhao, M., Cheng, L., Zhou, T., 2009. Direct numerical simulation of three-dimensional flow past a yawed circular cylinder of infinite length. *Journal of Fluids and Structures* 25, 831-847.